DOKUZ EYLÜL UNIVERSITY

GRADUATE SCHOOL OF NATURAL AND APPLIED SCIENCES

FAILURE ANALYSIS OF COMPOSITE LAMINATES CONTAINING THREE PIN LOADED HOLES

by

Özgür DEMİRGÖREN

February, 2007

İZMİR

FAILURE ANALYSIS OF COMPOSITE LAMINATES CONTAINING THREE PIN LOADED HOLES

A Thesis Submitted to the

Graduate School and Applied Sciences of Dokuz Eylül University

In Partial Fulfillment of the Requirements for the Degree of Master of Science

in Mechanical Engineering, Mechanics Program

by

Özgür DEMİRGÖREN

February, 2007

İZMİR

M.Sc. THESIS EXAMINATION RESULT FORM

We have read the thesis entitled **"FAILURE ANALYSIS OF COMPOSITE LAMINATES CONTAINING THREE PIN LOADED HOLES"** completed by **ÖZGÜR DEMİRGÖREN** under supervision of **Prof. Dr. RAMAZAN KARAKUZU** and we certify that in our opinion it is fully adequate, in scope and in quality, as a thesis for the degree of Master of Science.

Prof. Dr. Ramazan KARAKUZU

Supervisor

Prof. Dr. Onur SAYMAN

(Committee Member)

Yrd. Doç. Dr. Mustafa TOPARLI

(Committee Member)

Prof. Dr. Cahit Helvacı

Director

Graduate School of Natural and Applied Sciences

ACKNOWLEDGEMENTS

I would like to express my sincere gratitude to my supervisor, Prof. Dr. Ramazan KARAKUZU, for his excellent guidance, encouragement and patience throughout the preparation of this study.

I also would like to thank Prof. Dr. Onur SAYMAN for his academic support and encouragement through my M.Sc program.

I also extend my sincere thanks to research assistants Mr.Mehmet AKTAŞ, Mr.Cesim ATAŞ, Mr.B.Murat İÇTEN, Mr.Yusuf ARMAN and Mr.Faruk ŞEN for their help during both experimental and numerical phase of this study.

I also would like to thank to my colleagues of the members of "ARGE MEKANİK PROJELER YANSANAYİ GRUBU" for their support and tolerance.

And I would like to express my thanks to Özer TEKİNŞEN for his continous encouragement, support and friendship.

Finally, I am deeply grateful to my mother for her support, patience and understanding throughout my life.

Özgür DEMİRGÖREN

FAILURE ANALYSIS OF COMPOSITE LAMINATES CONTAINING THREE PIN LOADED HOLES

ABSTRACT

The aim of this investigation is to study the effect of different geometries on the failure behavior of glass-epoxy laminated composite plate which is subjected to a traction force by 3 rigid pins. The behavior of multi-pin loaded composite plates which have the stacking sequence of $[0/90/\pm45]_S$ and approx. 60% fiber volume fraction has been observed experimentally and numerically.

45 different geometries are used in this study by using 3 different hole distance parameters (The ratio of 'edge distance' to 'hole / pin diameter' E/D:1, 2, 3, 4, 5 ; The ratio of 'Longitudinal hole distance' to 'hole / pin diameter' F/D:2, 4, 6 ; The ratio of 'Transverse hole distance' to 'hole / pin diameter' G/D:3, 4, 5)

The three-dimensional finite element method was used to obtain stress distribution of the material. For analyzes, LUSAS 13.6 finite element analyze software has been used.. During the study geometric non-linear behavior and "Hashin Failure Criteria" have been selected to determine the "Failure Mode" and the "Failure Load".

The results of numerical and experimental study have been plotted and compared with each other.

Keywords: glass-epoxy composite, pin loading, failure mode, failure load

ÜÇ PİM İLE YÜKLENMİŞ TABAKALI KOMPOZİTLERDE HASAR ANALİZİ

ÖZ

Bu araştırmanın amacı 3 rijid pim ile çeki yükü uygulanmış cam lifi-epoksi kompozit plakasının farklı geometrilerinin hasar davranışına etkilerini incelemektir. $[0/90/\pm45]_S$ dizilimine sahip ve hacimce fiber yüzdesi yaklaşık %60 olan çoklu-pim yüklemeli kompozit plakaların davranışı deneysel ve nümerik olarak incelenmiştir.

Bu çalışmada 45 farklı geometri kullanılmış olup, 3 farklı delik mesafe parametresini(Kenar mesafesinin delik/pim çapına oranı E/D:1, 2, 3, 4, 5 ; Boylamasına delik mesafesinin delik/pim çapına oranı F/D:2, 4, 6 ; Enlemesine delik mesafesinin delik/pim çapına oranı G/D:3, 4, 5) içermektedir.

Malzemenin gerilme dağılımlarını elde etmek üzere üç boyutlu sonlu eleman metodu kullanıldı. Analizlerde LUSAS 13.6 sonlu eleman analiz yazılımı seçildi. Çalışma esnasında, "Hasar modu" ve "Hasar Yükü"nü belirlemek üzere lineer olmayan geometrik davranış ve "Hashin hasar kriteri" tercih edildi.

Nümerik ve deneysel çalışma sonuçları grafiğe aktarıldı ve kendi içlerinde karşılaştırıldı.

Anahtar Sözcükler: cam lifi-epoksi kompoziti, pimle yükleme, hasar modu, hasar yükü

CONTENTS

Page

CHAPTER ONE

INTRODUCTION

Composite material means that two or more materials are combined on a macroscopic scale to form a useful third material. Here, the key word is the macroscopic examination of a material wherein the components can be identified by the naked eye. Different materials can be combined on a microscopic scale, such as in alloying metals, but the resulting material is, for all practical purposes, macroscopically homogeneous, i.e., the components can not be identified by the naked eye and essentially act together. The advantage of composite materials is that, if well designed, they usually exhibit the best qualities of their components.

So composite materials are used in structures comprehensively where high mechanical performance is required and in designing ratio of high strength to weight takes care initially. Getting high strength and stiffness values while keeping weight in the low values provides the composites to take the place of metal materials used for the time immemorial.

In the structures made of composite laminates mechanical fasteners has a great importance at transferring loads and for this transaction a hole should be drilled on them. This holes cause stress concentration, inspite of these negativeness mechanical fasteners play an important role in airplane industry.

A non-appropriate joint design; causes low yielding although composites have a high level strength stress distribution over the hole wall should be considered straightly for sufficiently qualified strength evaluation and a realistic failure prediction.

Because of the anisotropic and heterogeneous nature of the composites joint problem analysis is much harder than the isotropic materials; separately owing to the unknown contact stresses and contact area between fastener and laminate, pin-loaded hole analysis is more complicated in comparison with free hole.

Chang (1984)a carried out analysis on T300/1034-C laminates has one pin-loaded hole and two pin-loaded holes (parallel; serial), never the less Chang (1984)b have developed a model and a computer code for composite laminates having a pin loaded hole to determine failure strength and failure mode , when the material exhibits non-linearly elastic behavior.

A large part of the literature published so far on mechanically-fastened joints present experimental results on the effect of the stacking sequence, geometric properties, clearance between the hole and the pin, and the degree of lateral clamping pressure exerted by the bolt. (Dano et al., 2000)

Lekhnitskii (1968) and later Savin (1968) analyzed problems related to the determination of the stress distribution in anisotropic plates weakened by an opening and deformed by forces applied to the mid plane.

Whitney and Nuismer (1974) introduced two related failure criteria: the point stress and the average stress failure criterion to evaluate the strength of composite plates containing through the thickness discontinuities.

Chang, Scott and Springer (1982) have developed a user-friendly computer code (designated as BOLT) which can be used to calculate the maximum load and which can be applied to joints involving fiber-reinforced laminates with different ply orientations, different material properties, and different configurations, including

different hole sizes, hole positions and thickness. They have used Yamada failure criterion.

Chang et al. (1984)a have extended their analysis to T300/1034-C laminates containing a pin-loaded hole or two pin-loaded holes in parallel or in series.

Chang et al. (1984)b have developed a model and corresponding computer code to determine failure strength and failure mode of composite laminates containing a pin loaded hole even when the material exhibits non-linearly elastic behavior.

Kretsis and Matthews (1985) showed that as the width of the specimen decreases, there is a point where the made of failure changes from one of bearing mode to one of tension mode, using E glass fiber-reinforced plastic and carbon fiber-reinforced plastic. A similar behavior between the end distance and the shear-out mode of failure was found. They concluded that lay-up had a great effect on both joint strength and failure mechanism. The bearing strength, failure load and failure modes are investigated in pin-loaded glass-vinylester laminated composite plate and the effects of changing the geometric parameters are observed. The three-dimensional finite element method is used to determine the failure load and failure mode using Hashin failure criteria. The mechanical properties of the laminated composite plate are obtained from standard tests.

Chen, Chiu and Chin (1994) have studied the influence of weave structure on pin-loaded strength of orthogonal 3D composites. They evaluated the influences of reinforcement type, weave structure, specimen width-to-diameter ratio and edge distance-to hole diameter ratio.

Larry and Mahmood (1995) have numerically investigated 2D progressive damage modeling of graphite epoxy composite pinned-joint failure. They analyzed

laminates that have different ply angle directions. In addition, they used fiber tensile-compressive, shearing, matrix tensile-compressive, and fiber-matrix shearing criteria. In their study, the specimens where the hole is located too close to the sides, W/D<3, or too close to the edge E/D<3, were characterized as weak.

Khashaba (1996) has conducted an experimental study to determine the notched and pin bearing strength of GFRP composites having various values of fiber volume fractions. The results show that fiber volume fraction has a significant effect on load-pin bearing displacement behavior and the value of W/D must be greater than 5 for the development of full bearing strength of the composite laminates.

A three dimensional finite element model to perform stress analysis of single and multi bolted double shear lap connections of glass fiber reinforced plastic has been used by Hassan et al. (1996) with using ANSYS program.

Mahmood and Larry (1996) have investigated non-linear three dimensional stress of pin-loaded composites which have $[0°_4/90°_4]_s$ and $[90°_4/0°_4]_s$ orientation ply angle.

Aktaş and Karakuzu (1998) have carried out failure load, failure mode, and propagation of failure in composite plate pinned-joints, both theoretically and experimentally.

Aktas and Karakuzu (1999) have carried out a failure analysis of mechanically fastened carbon-fiber reinforced epoxy composite plate of arbitrary orientation. In that work, failure load and failure mode have been analyzed experimentally and numerically using Tsai-Hill and fiber tensile-compressive failure criteria. They found that full bearing strength was developed when E/D and W/D ratios were equal to or greater than 4.

Camanho & Matthews (1999) have developed a 3D finite element model to predict damage progression and strength of mechanically fastened joints in carbon fibre reinforced plastics. To predict the failure mode, Hashin failure criteria has been used and compared with the experimental results.

Dahsin (1999) has investigated thickness effect of pinned joints for composites. He has studied the interaction between the pin diameter and composite thickness. Results show that thick composites with small pins and thin composites with large pins had lower efficiencies for joint stiffness and joint strength than those having similar dimensions between pin diameter and composite thickness.

Okutan, Aslan and Karakuzu (2001) have investigated the failure strength of pin-loaded woven fiber-glass reinforced epoxy laminates experimentally and have observed the effects of changing the with-to-hole diameter (W/D) and the ratio of edge distance to hole diameter (E/D) on the bearing strength of woven laminated composites. They have tested single-hole pin loaded specimens for their tensile response. They have observed failure propagation and failure type on the specimens.

Icten, Okutan and Karakuzu (2003) have investigated mechanical behaviour and damage development of pin-loaded woven glass fiber–epoxy composites, numerically and experimentally. To verify the numerical predictions of mechanical behaviour, a series of material configurations ($[(0/90)_3]_S$ _ $[(\pm45)_3]_S$) and 20 different geometries.

Khashaba et al. (2005) have investigated the influence of certain factors on the strength of bolted joints in $[0/\pm45/90]_s$ glass fiber reinforced epoxy (GFRE) composites. These factors were including the tightening torque and the washer outer diameter size. The mechanical properties (tensile, compressive, and in-plane shear) of GFRE laminates have been determined experimentally and theoretically. The experimental results showed that under the same tightening torque, the slope of load–

displacement diagrams of bolted joints (stiffness) increased with decreasing washer size.

Aktaş (2005) has carried out static and dynamic experimental studies to investigate both the static and dynamic bearing strengths of a pinned-joint carbon epoxy composite plate with $[0°/45°/-45°/90°]_s$ and $[90°/45°/-45°/0°]_s$ stacking configurations. The experiments showed that the static bearing strengths reach their upper limit when E/D and W/D ratios are equal to or greater than 4 for both [0°/ 45°/-45°/90°]s and [90°/45°/-45°/0°]s stacking sequences. The fatigue strength, on the other hand, reduced by up to 65% as E/D and W/D ratios increased for both stacking configurations.

Karakuzu et al. (2006)a have studied the bearing strength, failure mode and failure load in a woven laminated glass-vinylester composite plate with circular hole subjected to a traction force by a rigid pin. These are investigated for two variables; the distance from the free edge of the plate-to-the diameter of the hole (E/D) ratio (1, 2, 3, 4, 5), and the width of rectangular plate-to-the diameter of the hole (W/ D) ratio (2, 3, 4, 5), numerically and experimentally. Hashin failure criteria is used in the failure analysis.

Karakuzu et al. (2006)b have performed experimental and numerical study on the bearing strength, failure load and failure mode of pin loaded woven kevlar-epoxy plate was presented. In numerical study, Hashin, Hoffman and Maximum Stress failure criteria were used to predict the failure load and failure mode. Experimental results concerning damage progression and ultimate strength of the joint were obtained and compared with these predictions. To develop the full bearing strength the critical values of in-plane geometric parameters were investigated. In parametric studies, one of the variables was changed while the others are constant. It was seen that the results obtained numerically and experimentally are close to each other.

Wang et al. (2006) has carried out an experimental investigation to understand the bearing strength of stitched and unstitched uniweave T300/QY9512 laminates with single-lap single-bolt joint configuration. The objectives of the studies are to determine the effects of stitching node position, stacking sequence, and hygrothermal environment on the bearing strength and the load–displacement curves of stitched laminates. A three-dimensional finite element model is developed to investigate the bearing properties of mechanically fastened joints in unstitched and stitched laminates. Hashin's three-dimensional failure criterion is used to predict the progressive ply failure. The results showed that the bearing strength decreased when the stitching node position was close to the hole boundary.

The objective of this research is to study the failure behavior and investigate the effect of different geometries and different ply orientations of glass-epoxy laminated composite plate which is subjected to traction force by 3 rigid pins. The numerical and experimental studies implemented with particular attention given to the sensitivity of the model to different geometric dimensions. The three-dimensional finite element method was used to obtain stress distribution of the material. During the study “Hashin Failure Criteria” has been selected to determine the “Failure Mode” and the “Failure Load”. The mechanical properties of the composite material were obtained from the standard test methods.

CHAPTER TWO

STRUCTURAL ANALYSIS OF COMPOSITE MATERIALS

2.1 Classical Analysis

The use of classical methods of stress analysis has developed over many decades to give techniques that can be applied satisfactorily to a vast range of situations. Such analyses are based on the application of the equations of equilibrium and compatibility, together with the stress-strain relations for the material, to produce governing equations which must be solved to obtain displacements and stresses. Usually, assumptions must be made before a solution can be affected. So, for example, problems are considered as one-or two-dimensional, as when considering beams and plates, respectively. Often we take the material to be isotropic, but many analyses also exist for anisotropic materials.

When the mechanical properties of composites are calculated, it is convenient to start by considering a composite in which all the fibres are aligned in one direction (i.e. a unidirectional composite). This basic 'building block' can then be used to predict the behavior of continuous fibre multidirectional laminates, as well as short fibre, non-aligned systems.

The essential point about a unidirectional fibre composite is that its stiffness (and strength) are different in different directions. This behavior contrasts with a metal with a random orientation of grains, or other isotropic material, which has the same elastic properties in all directions.

In a unidirectional composite the fibre distribution implies that the behavior is essentially isotropic in a cross-section perpendicular to the fibres (Fig. 2.1). In other words, if we were to conduct a mechanical test by applying a stress in the '2' direction or in the '3' direction (both normal to the fibre's longitudinal axis), we would obtain the same elastic properties from each test. We say the material is 'transversely isotropic'. Clearly the properties in the longitudinal ('1') direction are very different from those in the other two directions. We call such a material 'orthotropic'. The elastic properties are symmetric with respect to the chosen (1-2-3) axes, which are usually called the 'principal material axes'.

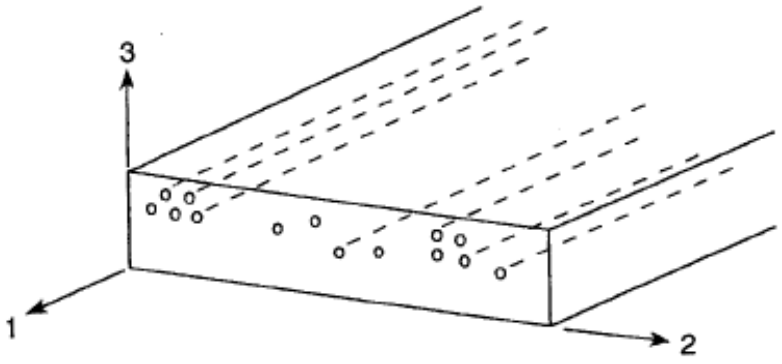

Figure 2.1 Orientation of principal material axes.

2.1.1 Basic Stress-Strain Relations

The stress-strain relations for the unidirectional material can readily be found, provided we take account of the fact that the properties are direction-dependent. Considering the composite illustrated in Fig. 2.1, we see that if the directions of the applied stresses coincide with the principal material axes (specially orthotropic), the strains in terms of the stresses are given by

$$\begin{Bmatrix} \varepsilon_1 \\ \varepsilon_2 \\ \varepsilon_3 \\ \gamma_{23} \\ \gamma_{31} \\ \gamma_{12} \end{Bmatrix} = \begin{bmatrix} S_{11} & S_{12} & S_{13} & 0 & 0 & 0 \\ S_{12} & S_{22} & S_{23} & 0 & 0 & 0 \\ S_{13} & S_{23} & S_{33} & 0 & 0 & 0 \\ 0 & 0 & 0 & S_{44} & 0 & 0 \\ 0 & 0 & 0 & 0 & S_{55} & 0 \\ 0 & 0 & 0 & 0 & 0 & S_{66} \end{bmatrix} \begin{Bmatrix} \sigma_1 \\ \sigma_2 \\ \sigma_3 \\ \tau_{23} \\ \tau_{31} \\ \tau_{12} \end{Bmatrix} \tag{2.1}$$

where,

$$S_{11} = \frac{1}{\mathrm{E}_1},\ S_{12} = -\frac{\nu_{12}}{\mathrm{E}_1} = -\frac{\nu_{21}}{\mathrm{E}_2},\ S_{13} = -\frac{\nu_{13}}{\mathrm{E}_1} = -\frac{\nu_{31}}{\mathrm{E}_3},\ S_{23} = -\frac{\nu_{23}}{\mathrm{E}_2} = -\frac{\nu_{32}}{\mathrm{E}_3}$$

$$S_{22} = \frac{1}{\mathrm{E}_2},\ S_{33} = \frac{1}{\mathrm{E}_3},\ S_{44} = \frac{1}{G_{23}},\ S_{55} = \frac{1}{G_{31}},\ S_{66} = \frac{1}{G_{12}} \tag{2.2}$$

The strain-stress relations in Eq. 2.1 can be inverted to obtain the stress-strain relations:

$$\begin{Bmatrix} \sigma_1 \\ \sigma_2 \\ \sigma_3 \\ \tau_{23} \\ \tau_{31} \\ \tau_{12} \end{Bmatrix} = \begin{bmatrix} C_{11} & C_{12} & C_{13} & 0 & 0 & 0 \\ C_{12} & C_{22} & C_{23} & 0 & 0 & 0 \\ C_{13} & C_{23} & C_{33} & 0 & 0 & 0 \\ 0 & 0 & 0 & C_{44} & 0 & 0 \\ 0 & 0 & 0 & 0 & C_{55} & 0 \\ 0 & 0 & 0 & 0 & 0 & C_{66} \end{bmatrix} \begin{Bmatrix} \varepsilon_1 \\ \varepsilon_2 \\ \varepsilon_3 \\ \gamma_{23} \\ \gamma_{31} \\ \gamma_{12} \end{Bmatrix} \tag{2.3}$$

The stiffness matrix, C_{ij}, for an orthotropic material in terms of the engineering constants, is obtained by inversion of the compliance matrix, S_{ij}. The stiffness' in Eq. (2.3) are

$$C_{11} = \frac{1-\upsilon_{23}\upsilon_{32}}{E_2E_3\Delta},\ C_{22} = \frac{1-\upsilon_{13}\upsilon_{31}}{E_1E_3\Delta},\ C_{12} = \frac{\upsilon_{21}+\upsilon_{31}\upsilon_{23}}{E_2E_3\Delta} = \frac{\upsilon_{12}+\upsilon_{32}\upsilon_{13}}{E_1E_3\Delta}$$

$$C_{23} = \frac{\upsilon_{32}+\upsilon_{12}\upsilon_{31}}{E_1E_3\Delta} = \frac{\upsilon_{23}+\upsilon_{21}\upsilon_{13}}{E_1E_2\Delta},\ C_{13} = \frac{\upsilon_{31}+\upsilon_{21}\upsilon_{32}}{E_2E_3\Delta} = \frac{\upsilon_{13}+\upsilon_{12}\upsilon_{23}}{E_1E_2\Delta} \tag{2.4}$$

$$C_{33} = \frac{1-\upsilon_{12}\upsilon_{21}}{E_1E_2\Delta},\ C_{44} = G_{23},\ C_{55} = G_{31},\ C_{66} = G_{12}$$

where,

$$\Delta = \frac{1-\upsilon_{12}\upsilon_{21}-\upsilon_{23}\upsilon_{32}-\upsilon_{31}\upsilon_{13}-2\upsilon_{21}\upsilon_{32}\upsilon_{13}}{E_1E_2E_3} \tag{2.5}$$

The principal directions of orthotropy often do not coincide with coordinate directions that are geometrically natural to the solution of the problem. For this reason, a method of transforming stress-strain relations from one coordinate system to another is needed.

The principal material axes and θ, is the angle from the *x* axis to 1 axis, are shown in Figure 2.2.

The stress transformations between x-y-z and 1-2-3 are,

$$\begin{Bmatrix} \sigma_{xx} \\ \sigma_{yy} \\ \sigma_{zz} \\ \sigma_{yz} \\ \sigma_{xz} \\ \sigma_{xy} \end{Bmatrix} = \begin{bmatrix} \cos^2\theta & \sin^2\theta & 0 & 0 & 0 & -\sin 2\theta \\ \sin^2\theta & \cos^2\theta & 0 & 0 & 0 & \sin 2\theta \\ 0 & 0 & 1 & 0 & 0 & 0 \\ 0 & 0 & 0 & \cos\theta & \sin\theta & 0 \\ 0 & 0 & 0 & -\sin\theta & \cos\theta & 0 \\ \sin\theta\cos\theta & -\sin\theta\cos\theta & 0 & 0 & 0 & \cos^2\theta-\sin^2\theta \end{bmatrix} \begin{Bmatrix} \sigma_1 \\ \sigma_2 \\ \sigma_3 \\ \sigma_4 \\ \sigma_5 \\ \sigma_6 \end{Bmatrix} \tag{2.6}$$

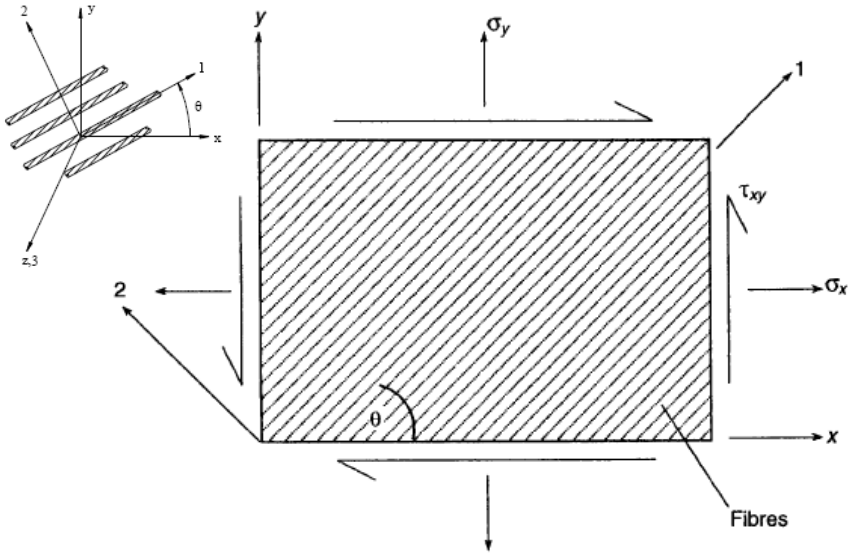

Figure 2.2 Unidirectional lamina with principal axes rotating by θ relative to the ***x-y*** axes

The strain-stress relations in x-y-z coordinates are;

$$\begin{Bmatrix} \varepsilon_{xx} \\ \varepsilon_{yy} \\ \varepsilon_{zz} \\ \gamma_{yz} \\ \gamma_{xz} \\ \gamma_{xy} \end{Bmatrix} = \begin{bmatrix} \overline{S}_{11} & \overline{S}_{12} & \overline{S}_{13} & 0 & 0 & \overline{S}_{16} \\ \overline{S}_{12} & \overline{S}_{22} & \overline{S}_{23} & 0 & 0 & \overline{S}_{26} \\ \overline{S}_{13} & \overline{S}_{23} & \overline{S}_{33} & 0 & 0 & \overline{S}_{36} \\ 0 & 0 & 0 & \overline{S}_{44} & \overline{S}_{45} & 0 \\ 0 & 0 & 0 & \overline{S}_{45} & \overline{S}_{55} & 0 \\ \overline{S}_{16} & \overline{S}_{26} & \overline{S}_{36} & 0 & 0 & \overline{S}_{66} \end{bmatrix} \begin{Bmatrix} \sigma_{xx} \\ \sigma_{yy} \\ \sigma_{zz} \\ \sigma_{yz} \\ \sigma_{xz} \\ \sigma_{xy} \end{Bmatrix} \tag{2.7}$$

The transformed compliance coefficients S_{ij} , referred to the (x, y, z) system,

$$\overline{S}_{11} = S_{11}\cos^4\theta - 2S_{16}\cos^3\theta\sin\theta + (2S_{12} + S_{66})\cos^2\theta\sin^2\theta - 2S_{26}\cos\theta\sin^3\theta + S_{22}\sin^4\theta$$

$$\overline{S}_{12} = S_{12}\cos^4\theta - (S_{16} - S_{26})\cos^3\theta\sin\theta + (S_{11} + S_{22} - S_{66})\cos^2\theta\sin^2\theta + (S_{26} - S_{16})\cos\theta\sin^3\theta + S_{12}\sin^4\theta$$

$$\overline{S}_{13} = S_{13}\cos^2\theta - S_{36}\cos\theta\sin\theta + S_{23}\sin^2\theta$$

$$\overline{S}_{16} = S_{16}\cos^4\theta + (2S_{11} - 2S_{12} - S_{66})\cos^3\theta\sin\theta + 3(S_{26} - S_{16})\cos^2\theta\sin^2\theta + (S_{66} + 2S_{12} - 2S_{22})\cos\theta\sin^3\theta + S_{26}\sin^4\theta$$

$$\overline{S}_{22} = S_{22}\cos^4\theta + 2S_{26}\cos^3\theta\sin\theta + (2S_{12} + S_{66})\cos^2\theta\sin^2\theta + 2S_{16}\cos\theta\sin^3\theta + S_{11}\sin^4\theta$$

$$\overline{S}_{23} = S_{23}\cos^2\theta + S_{36}\cos\theta\sin\theta + S_{13}\sin^2\theta$$

$$\overline{S}_{26} = S_{26}\cos^4\theta + (2S_{12} - 2S_{22} + S_{66})\cos^3\theta\sin\theta + 3(S_{16} - S_{26})\cos^2\theta\sin^2\theta + (2S_{11} - 2S_{12} - S_{66})\cos\theta\sin^3\theta - S_{16}\sin^4\theta$$

$$\overline{S}_{33} = S_{33}$$

$$\overline{S}_{36} = 2(S_{13} - S_{23})\cos\theta\sin\theta + S_{36}(\cos^2\theta - \sin^2\theta)$$

$$\overline{S}_{44} = S_{44}\cos^2\theta + 2S_{45}\cos\theta\sin\theta + S_{55}\sin^2\theta$$

$$\overline{S}_{45} = S_{45}(\cos^2\theta - \sin^2\theta) + (S_{55} - S_{44})\cos\theta\sin\theta$$

$$\overline{S}_{55} = S_{55}\cos^2\theta - 2S_{45}\cos\theta\sin\theta + S_{44}\sin^2\theta$$

$$\overline{S}_{66} = S_{66}(\cos^2\theta - \sin^2\theta) + 4(S_{16} - S_{26})(\cos^2\theta - \sin^2\theta)\cos\theta\sin\theta + 4(S_{11} + S_{22} - 2S_{12})\cos^2\theta\sin^2\theta \tag{2.8}$$

The stress-strain relations in x-y-z coordinates are,

$$\begin{Bmatrix} \sigma_{xx} \\ \sigma_{yy} \\ \sigma_{zz} \\ \sigma_{yz} \\ \sigma_{xz} \\ \sigma_{xy} \end{Bmatrix} = \begin{bmatrix} \overline{C}_{11} & \overline{C}_{12} & \overline{C}_{13} & 0 & 0 & \overline{C}_{16} \\ \overline{C}_{21} & \overline{C}_{22} & \overline{C}_{23} & 0 & 0 & \overline{C}_{26} \\ \overline{C}_{31} & \overline{C}_{32} & \overline{C}_{33} & 0 & 0 & \overline{C}_{36} \\ 0 & 0 & 0 & \overline{C}_{44} & \overline{C}_{45} & 0 \\ 0 & 0 & 0 & \overline{C}_{45} & \overline{C}_{55} & 0 \\ \overline{C}_{16} & \overline{C}_{26} & \overline{C}_{36} & 0 & 0 & \overline{C}_{66} \end{bmatrix} \begin{Bmatrix} \varepsilon_{xx} \\ \varepsilon_{yy} \\ \varepsilon_{zz} \\ \gamma_{yz} \\ \gamma_{xz} \\ \gamma_{xy} \end{Bmatrix} \tag{2.9}$$

The transformed compliance coefficients C_{ij} , referred to the (x, y, z) system,

$$\overline{C}_{11} = C_{11}\cos^4\theta - 4C_{16}\cos^3\theta\sin\theta + (2C_{12} + C_{66})\cos^2\theta\sin^2\theta - 4C_{26}\cos\theta\sin^3\theta + C_{22}\sin^4\theta$$

$$\overline{C}_{12} = C_{12}\cos^4\theta + 2(C_{16} - C_{26})\cos^3\theta\sin\theta + (C_{11} + C_{22} - 4C_{66})\cos^2\theta\sin^2\theta + 2(C_{26} - C_{16})\cos\theta\sin^3\theta + C_{12}\sin^4\theta$$

$$\overline{C}_{13} = C_{13}\cos^2\theta - 2C_{36}\cos\theta\sin\theta + C_{23}\sin^2\theta$$

$$\overline{C}_{16} = C_{16}\cos^4\theta + (C_{11} - C_{12} - 2C_{66})\cos^3\theta\sin\theta + 3(C_{26} - C_{16})\cos^2\theta\sin^2\theta + (2C_{66} + C_{12} - C_{22})\cos\theta\sin^3\theta - C_{26}\sin^4\theta$$

$$\overline{C}_{22} = C_{22}\cos^4\theta + 4C_{26}\cos^3\theta\sin\theta + 2(C_{12} + 2C_{66})\cos^2\theta\sin^2\theta + 4C_{16}\cos\theta\sin^3\theta + C_{11}\sin^4\theta$$

$$\overline{C}_{23} = C_{23}\cos^2\theta + 2C_{36}\cos\theta\sin\theta + C_{13}\sin^2\theta$$

$$\overline{C}_{26} = C_{26}\cos^4\theta + (C_{12} - C_{22} + 2C_{66})\cos^3\theta\sin\theta + 3(C_{16} - C_{26})\cos^2\theta\sin^2\theta + (C_{11} - C_{12} - 2C_{66})\cos\theta\sin^3\theta - C_{16}\sin^4\theta$$

$$\overline{C}_{33} = C_{33}$$

$$\overline{C}_{36} = (C_{13} - C_{23})\cos\theta\sin\theta + C_{36}(\cos^2\theta - \sin^2\theta)$$

$$\overline{C}_{44} = C_{44}\cos^2\theta + 2C_{45}\cos\theta\sin\theta + C_{55}\sin^2\theta$$

$$\overline{C}_{45} = C_{45}(\cos^2\theta - \sin^2\theta) + (C_{55} - C_{44})\cos\theta\sin\theta$$

$$\overline{C}_{55} = C_{55}\cos^2\theta - 2C_{45}\cos\theta\sin\theta + C_{44}\sin^2\theta$$

$$\overline{C}_{66} = 2(C_{16} - C_{26})\cos^3\theta\sin\theta + (C_{11} + C_{22} - 2C_{12} - 2C_{66})\cos^2\theta\sin^2\theta + 2(C_{26} - C_{16})\cos\theta\sin^3\theta + C_{66}(\cos^4\theta + \sin^4\theta) \qquad (2.10)$$

Note that C_{14}, C_{15}, C_{16}, C_{24}, C_{25}, C_{26}, C_{34}, C_{35}, C_{36}, C_{45}, C_{46}, and C_{56} are zero for an orthotropic material.

2.2 Finite Element Analysis:

Finite Element (FE) analysis is merely an alternative approach to solving the governing equations of a structural problem. Hence, FE and classical methods will produce identical results for the same problem, provided the former method is correctly applied.

The method consists of imagining the structure to be composed of discrete parts (i.e. finite elements), which are then assembled in such way as to represent the distortion of the structure under the specified loads. Each element has an assumed displacement field, and part of the skill of applying the method is in selecting appropriate elements of the correct size and distributions (the FE 'mesh').

The FE method was initially developed for isotropic materials and the majority of elements available (the 'library') in any software package would be for such materials. To apply the technique to composites requires different element formulations that adequately represent their anisotropic, or orthotropic, stiffness and strength, as well as the laminated form of construction often used.

2.2.1 Three-Dimensional Finite Element Method

In the three-dimensional finite element formulation, the displacements, traction components, and distributed body force values are the functions of the position indicated by (x, y, z). The displacement vector $\mathbf{u}$ is given as

$$\mathbf{u} = (u,v,w)^T \tag{2.19}$$

where *u,* ν and w are the *x, y* and *z* components of **u**, respectively. The stress and strains are given by

$$\sigma = \left[\sigma_{xx}, \sigma_{yy}, \sigma_{zz}, \sigma_{yz}, \sigma_{xz}, \sigma_{xy}\right]^T$$
$$\varepsilon = \left[\varepsilon_{xx}, \varepsilon_{yy}, \varepsilon_{zz}, \gamma_{yz}, \gamma_{xz}, \gamma_{xy}\right]^T \tag{2.20}$$

From Figure 2.6, representing the three- dimensional problem in a general setting, the body force and traction vector are given by

$$\mathbf{f} = [\, f_x, f_y, f_z \,]^T \;, \quad \mathbf{T} = [\, T_x, T_y, T_z \,]^T \tag{2.21}$$

The body force **f** has dimensions of force per unit volume, while the traction force **T** has dimensions of force per unit area.

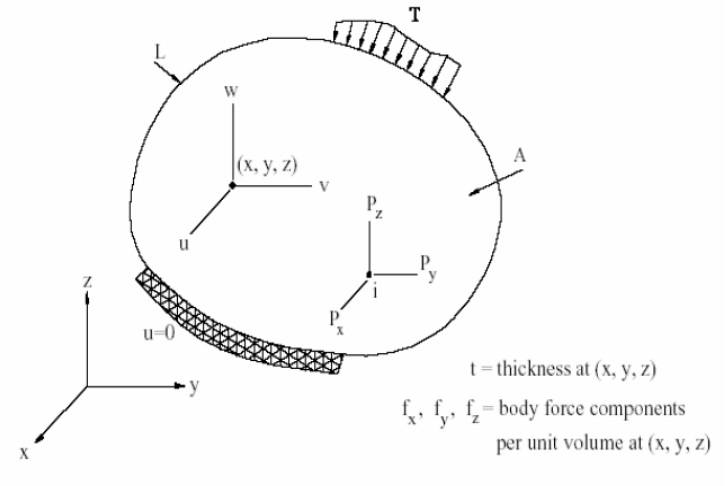

Figure 2.6 Three dimensional problem

2.2.2 The sixteen-Node Brick Element

The sixteen-node brick element is a simple three-dimensional element used in the analysis of solid mechanics problem. A 3D isoparametric solid continuum element capable of modeling curved boundaries. The element is numbered according to right-hand screw rule in the local z-direction. Freedoms of the element are u, v, w at each node and node coordinates are x, y, z at each node. A typical sixteen-node brick element is shown in Figure 2.7

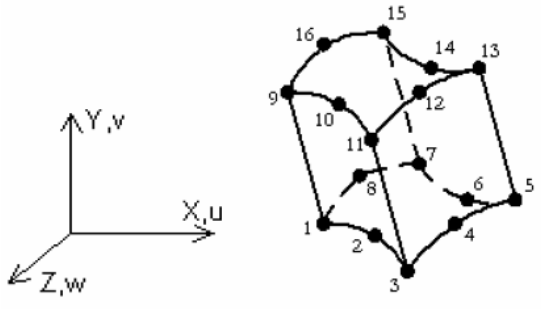

Figure 2.7 Sixteen-node brick element

Hashin failure criteria (1980) are polynomial failure criteria similar to the quadratic failure envelope except that in the Hashin formulation there are distinct polynomials corresponding to the different modes. Hashin-type failure criteria are ideal for use in finite element models, especially when adapted to progressive damage models. Hashin proposed a set of failure criteria for predicting failure of unidirectional composites based on each failure mode.

Tensile Fiber Mode:

$$\left(\frac{\sigma_{11}}{X_T}\right)^2 + \frac{1}{S^2}(\sigma_{12}{}^2 + \sigma_{13}{}^2) = 1$$

or

$$\sigma_{11} = X_T \tag{2.22}$$

Compressive Fiber Mode:

$$|\sigma_{11}| = X_c \tag{2.23}$$

Tensile Matrix Mode: $(\sigma_{22} + \sigma_{33}) > 0$

$$\frac{1}{Y_T{}^2}(\sigma_{22} + \sigma_{33})^2 + \frac{1}{S_T{}^2}(\sigma_{33}{}^2 - \sigma_{22}\sigma_{33}) + \frac{1}{S^2}(\sigma_{12}{}^2 + \sigma_{13}) = 1 \tag{2.24}$$

Compressive Matrix Mode:

$$\frac{1}{Y_c{}^2}\left[\left(\frac{Y_c}{2S_T}\right) - 1\right](\sigma_{22} + \sigma_{33}) + \frac{1}{4S_T{}^2}(\sigma_{22} + \sigma_{33})^2 + \frac{1}{S_T{}^2}(\sigma_{23}{}^2 - \sigma_{22}\sigma_{33}) + \frac{1}{S^2}(\sigma_{12}{}^2 + \sigma_{13}{}^2) = 1 \tag{2.25}$$

where;

σ_{11} is the normal stress in the direction of the fibers of the lamina.

σ_{22}, σ_{33} are the normal stresses in the transverse directions to the fibers of the lamina.

σ_{23}, σ_{13}, σ_{12} are the shear stresses in the lamina.

X_T is the tensile strength of the fibers.

X_C is the compressive strength of the fibers.

Y_T is the tensile strength in the transverse direction of the fibers.

Y_C is the compression strength in the transverse direction of the fibers.

S is the shear strength, in the 1-2 plane of the lamina.

S_T is the transverse shear strength in the 1-3 and 2-3 planes of the lamina.

CHAPTER THREE

NUMERICAL STUDY

3.1 Objective

The objective of the numerical study is to determine the failure loads and failure modes of the composite plates considered in experimental analysis and compare the results with the each other.

3.2 Explanation of the Numerical Study:

The numerical studies have been carried out by LUSAS 13.6 finite element analysis software. All of the specimens with different pin-configurations have been modeled and analyzed so that the failure loads have been determined.

Specimens modeled as a half model and symmetry boundary conditions were used to reduce the size of the model and calculation time.

While modeling meshes were graded manually by specifying the number of elements on each of the boundary lines. (See Figure 3.1)

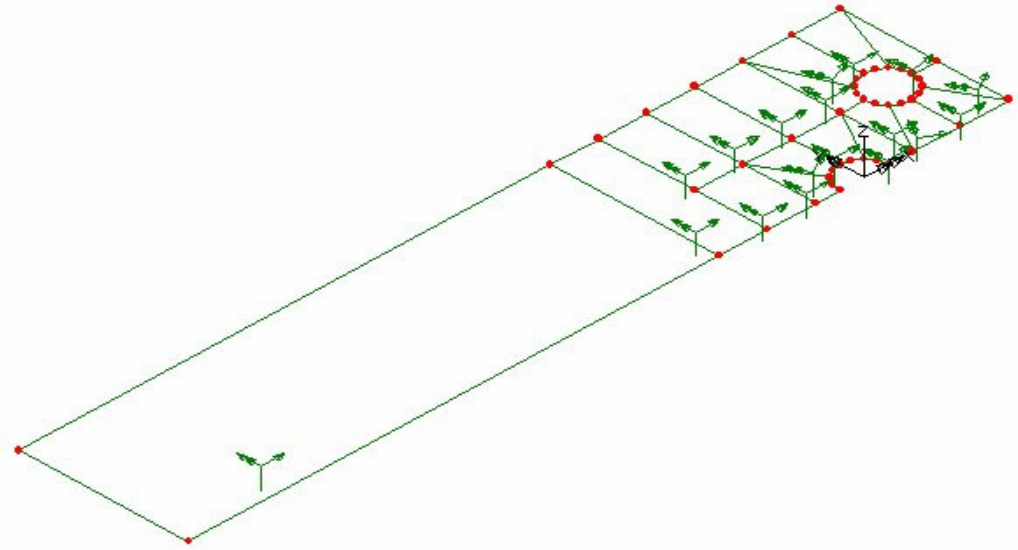

Figure 3.1 Modeling of the surfaces

After creating the surfaces, they were swept through the depth of the plate to create a volume. Then the mesh dataset Composite Brick (HX16L) were assigned to the volume. (See Figure 3.2)

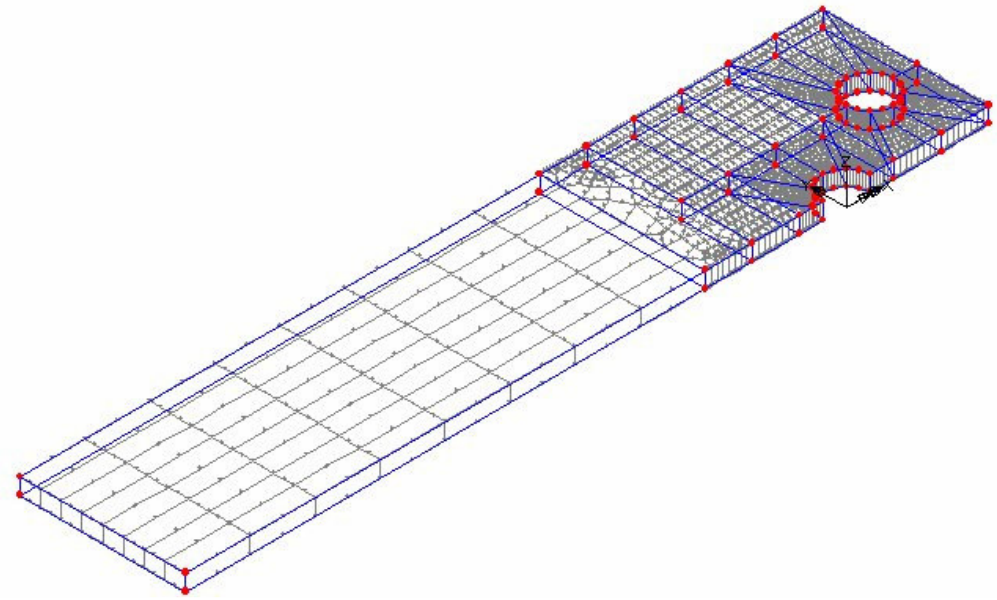

Figure 3.2 Composite Brick (HX16L) meshes.

After defining the material properties of glass-epoxy composite material indicated in Table 4.1, the ply orientations and stacking sequence of the composite plate, the boundary conditions and distributed load were defined.

The first boundary condition was the bottom surface of the symmetrically half model. It was defined as supported on xz plane.

The second boundary condition was the supporting face of the holes. These faces have been defined to support the load by cylindrical coordinates just like the bearing load, and they've been defined as fixed x direction support for the both holes.

Finally a distributed load was defined to the loading direction (x) of the model and after defining the failure criteria values, the analyses were carried out as geometric non-linear. (See Figure 3.3 & Figure 3.4)

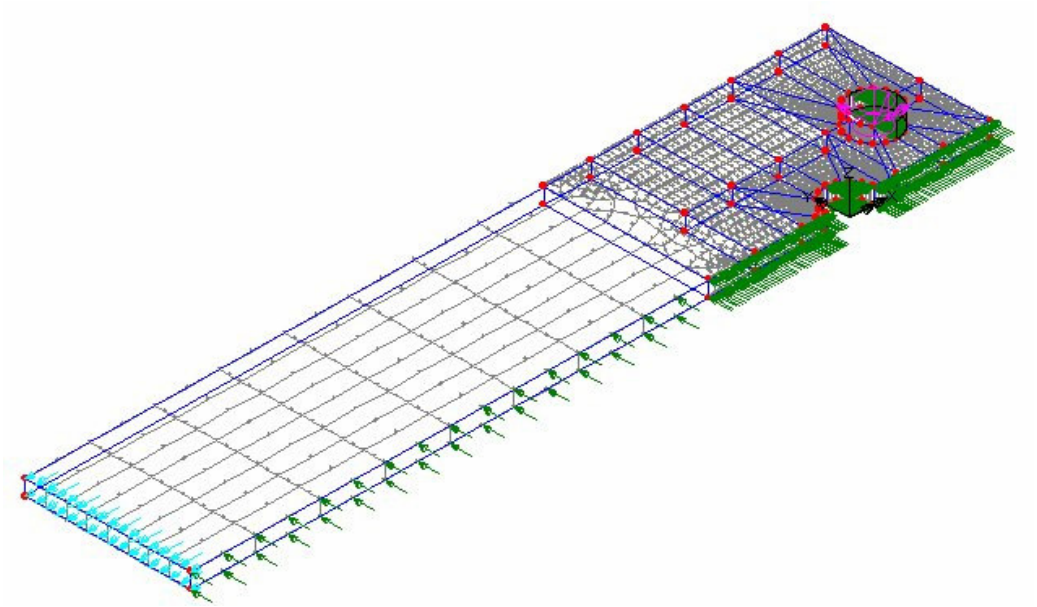

Figure 3.3 Boundary conditions of the model.

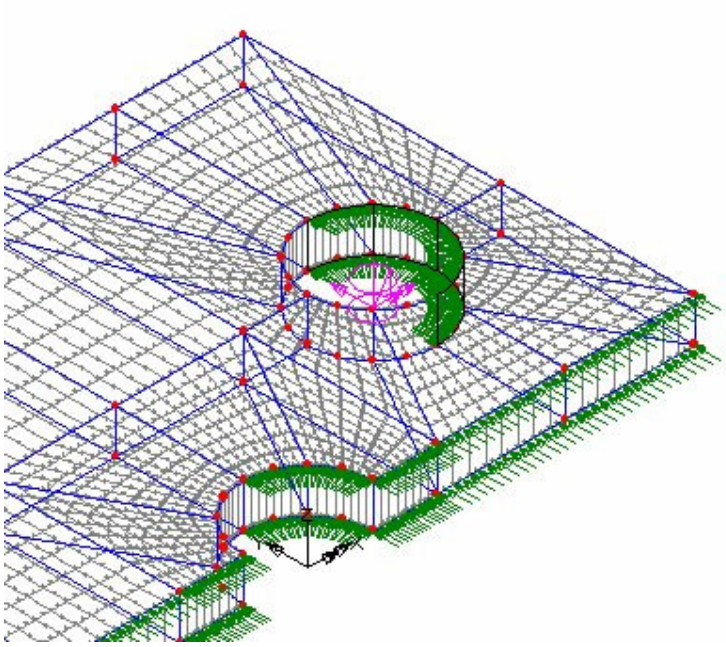

Figure 3.4 Boundary conditions of the model.

For the analyses, “geometric non-linear analyze method” and “Hashin Failure Criteria” were selected.

For each analyzed pin-configuration, failure loads have been determined and the stress contours have been plotted.

CHAPTER FOUR

EXPERIMENTAL STUDY

4.1 Objective

The objective of this research is to investigate the effect of failure behavior of multi-pinned-joint in glass-epoxy laminated composite plate. The experimental studies have been implemented as two set of tests. The purpose of the first set of test was to determine the material properties. The second set of was implemented to determine the "Failure Modes" and the "Failure Loads" of the laminates with different hole/pin combinations.

4.2 Problem Statement and Experimental Details

The configuration and loading studied in this research are shown in Figure 4.1 and Figure 4.2. A uniform tensile load P was applied to the test plate which was supported by 3 rigid pins with different arrangements. Load was parallel to the plate and symmetric with respect to the centerline so that it can not create bending moments about x, y, z axes.

The laminates with stacking arrangements of $[0/90/\pm45]_S$ were selected to investigate. (The 0° direction in the stacking notation denotes the x-axis or longitudinal direction.) The fiber-volume fraction of the composite is approximately 60%. The thickness of the material is 1.7 mm.

The geometry of test specimens is symmetrical about the y axes. (See Fig. 4.1)

The 45 different geometries were used so that a variety of failure modes and failure strength could be observed.

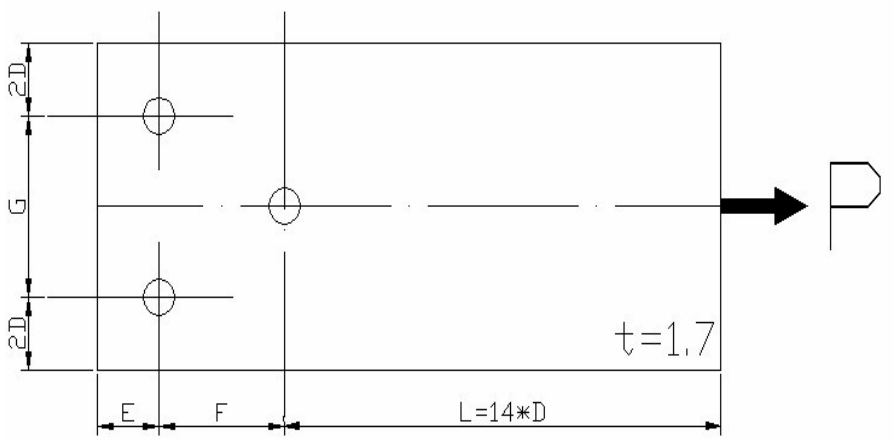

Figure 4.1 Geometry of test plates with 3 circular hole

The main parameters of the test plate can be described as follows:

- **L** – The length of the plate
- **D** – Hole / pin diameter
- **E** – Edge distance, the distance from the center of the holes to the free edge.
- **F** – Longitudinal hole distance
- **G** – Transverse hole distance, the distance between the holes along the transverse axis
- **E/D –** The ratio of 'edge distance' to 'hole / pin diameter', it has been varied as 1, 2, 3, 4, 5 in the study.
- **F/D –** The ratio of 'Longitudinal hole distance' to 'hole / pin diameter', it has been varied as 2, 4, 6 in the study.

- **G/D –** The ratio of 'Transverse hole distance' to 'hole / pin diameter', it, has been varied as 3, 4, 5 in the study.

There are, in general, three basic joint failure modes related to composite failure: net-tension, shear out and bearing, although, in practice, combinations of these failure modes are possible. Typical damages due to each mechanism are shown in Figure 4.2. Especially, the appearance of the net-tension failure is catastrophic, immediate and without warning. Therefore, the designer should choose optimal pin arrangements to avoid such catastrophic and immediate failure at structural elements in practical applications. (Okutan et al. 2001)

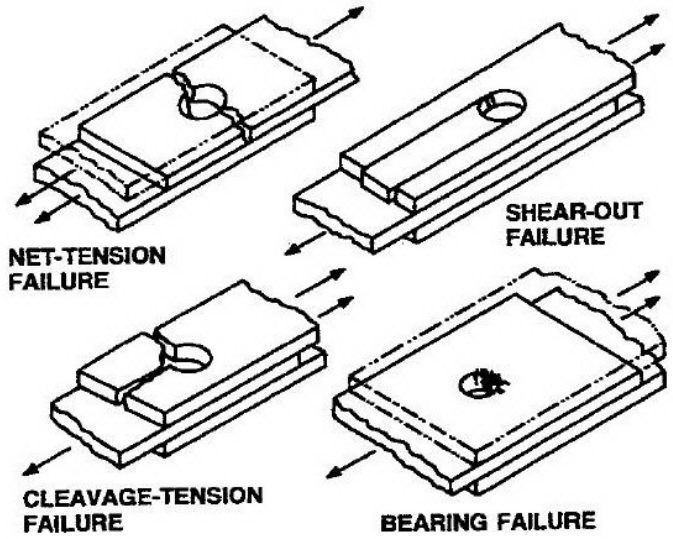

Figure 4.2 Typical failure mechanisms of the pinned-joint configuration (Jones, 1999)

4.3 Determination of Mechanical Properties

The elasticity modulus in direction of the fibers, E_1, and the Poisson's ratio ν_{12} can be determined by means of tension tests on unidirectional coupons that instrumented with electric resistance strain gages, as shown in Figure 4.3. One of them was placed to the fiber direction and the other one in the matrix direction.

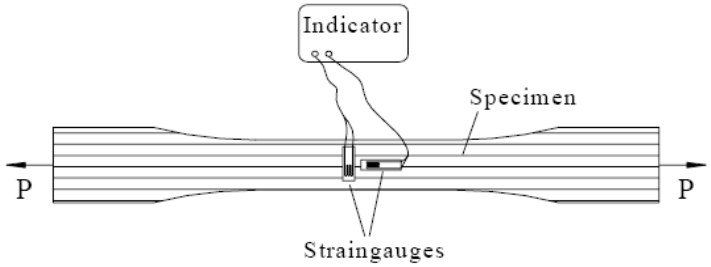

Figure 4.3 Test specimen for determination of E_1 and ν_{12}

The specimen which has the dimensions 150 mm x 12 mm x 1.7 mm was loaded step by step up to rapture by tensile test machine. For all steps, P, ε_1 and ε_2 values were measured.

Then, ν_{12} and E_1 were calculated by using the equations (4.1)

$$\sigma_1 = \frac{P}{A},\ \upsilon_{12} = -\frac{\varepsilon_2}{\varepsilon_1}, E_1 = \frac{\sigma_1}{\varepsilon_1} \tag{4.1}$$

The similar test was performed to determine E_2. The specimen which has the dimensions 150 mm x 25.6 mm x 1.7 mm was loaded step by step to rapture by tensile test machine. For all steps, *P*, ε_1 and ε_2 values were measured. (Figure 4.4)

Then, E_2 was calculated by using the equations (4.2)

$$\sigma_2 = \frac{P}{A},\ E_2 = \frac{\sigma_2}{\varepsilon_2} \tag{4.2}$$

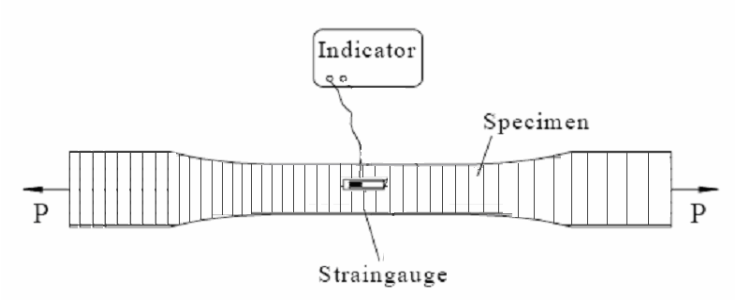

Figure 4.4 Test specimen for determination of E_2

To find $X_{t,}$ a specimen which has the dimensions 300 mm x 12 mm x 1.7 mm was loaded step by step to rapture by tensile test machine. (Figure 4.5) It was calculated from the equation (4.3)

$$X_t = \frac{P_{ult}}{A} \tag{4.3}$$

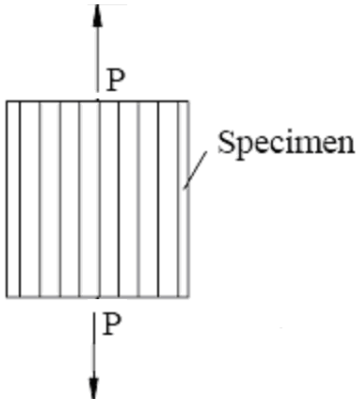

Figure 4.5 Longitudinal tension test

The similar test method was used to determine Y_t (Figure 4.6). The specimen dimensions were 300 mm x 25.6 mm x 1.7 mm. The Y_t value was calculated by the equation (4.4).

$$Y_t = \frac{P_{ult}}{A} \tag{4.4}$$

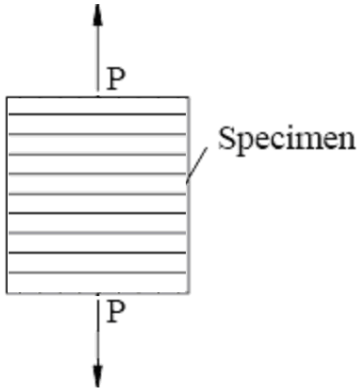

Figure 4.6 Transversal tension test

To find X_c, a specimen, which has the dimensions 7.5 mm x 1.7 mm and whose fiber direction coincides with the loading direction was taken and it was subjected to compressive loading (Fig.4.7). X_c was also calculated by dividing the ultimate force by the cross-sectional area of the specimen. (Equation (4.5))

$$X_c = \frac{P_{ult}}{A} \tag{4.5}$$

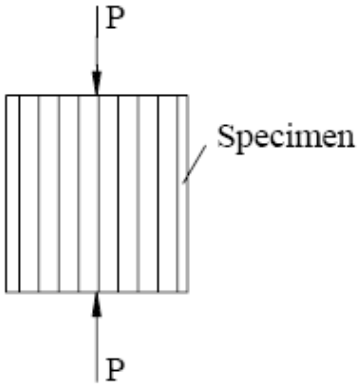

Figure 4.7 Longitudinal compression test

The similar test method was used to determine Y_c. (Figure 4.8) The specimen dimensions were 7.5 mm x 1.7 mm. The value was calculated by the equation (4.6).

$$Y_c = \frac{P_{ult}}{A} \tag{4.6}$$

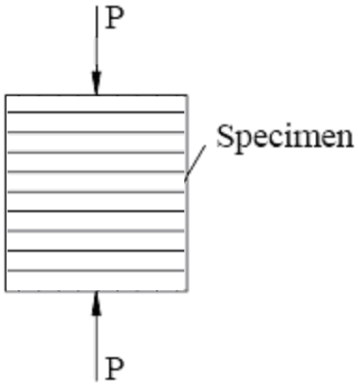

Figure 4.8 Transversal compression test

To define the shear modulus G_{12}, a specimen whose principal axis was on 45° was taken and a strain gauge was stuck on loading direction of the lamina (Fig.4.9). The specimen was loaded step by step up to rapture by the test machine and G_{12} was calculated by measurement of the strain in the tensile direction ε_x.

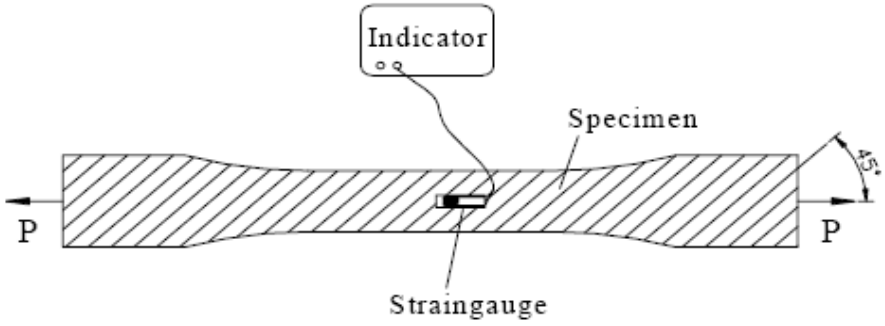

Figure 4.9 Shear Test

$$E_x = \frac{P/A}{\varepsilon_x}$$
$$G_{12} = \frac{1}{\frac{4}{E_x} - \frac{1}{E_1} - \frac{1}{E_2} + \frac{2\upsilon_{12}}{E_1}} \tag{4.7}$$

Iosipescu testing method was used to define the shear strength *S* (Fig.5.10). The dimensions of the specimen were chosen as; L=80 mm, h=20 mm, w=12 mm and t_i=1.7 mm. A compression test was applied to the specimen. In failure, S was calculated from

$$S = \frac{P_{\max}}{t_i c} \tag{4.5}$$

where P_{max} is the failure force.

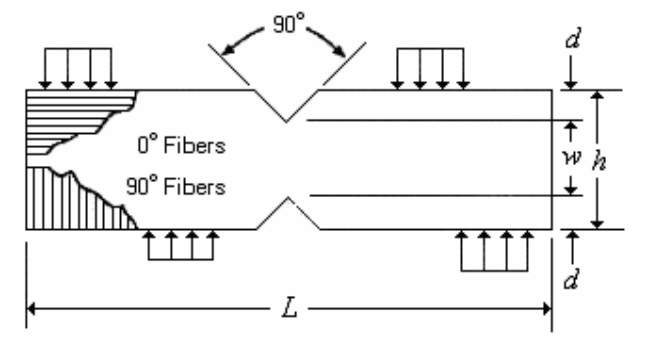

(a)

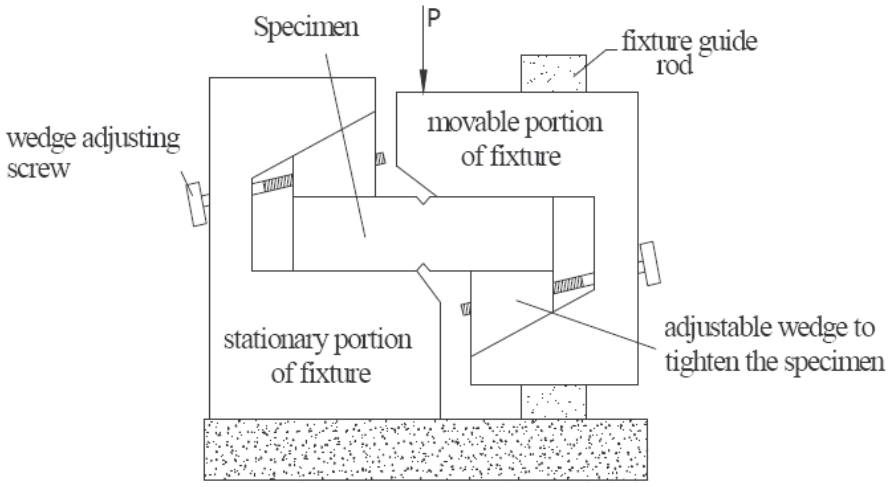

(b)

Figure 4.10. (a) Iosipescu test specimen, (b) Iosipescu test specimen and testing fixture

The mechanical properties of glass/epoxy composite plate which were obtained from the experimental study have been given in Table 4.1.

Table 4.1 Mechanical properties of glass/epoxy

E_1 (GPa)	E_2 (GPa)	G_{12} (GPa)	ν_{12}	X_c (MPa)	Y_c (MPa)	X_t (MPa)	Y_t (MPa)	S (MPa)
37.461	7.998	3.965	0.2725	223.37	109.01	686.77	73.88	78.59

Experiments were carried out in tension mode with the tensile machine. The lower edge of the specimen clamped and loaded from the steel pins by stretching the specimens at a ratio 0.5 mm/mm (Figure 4.11). The load – pin displacement diagrams for all composite configurations were plotted.

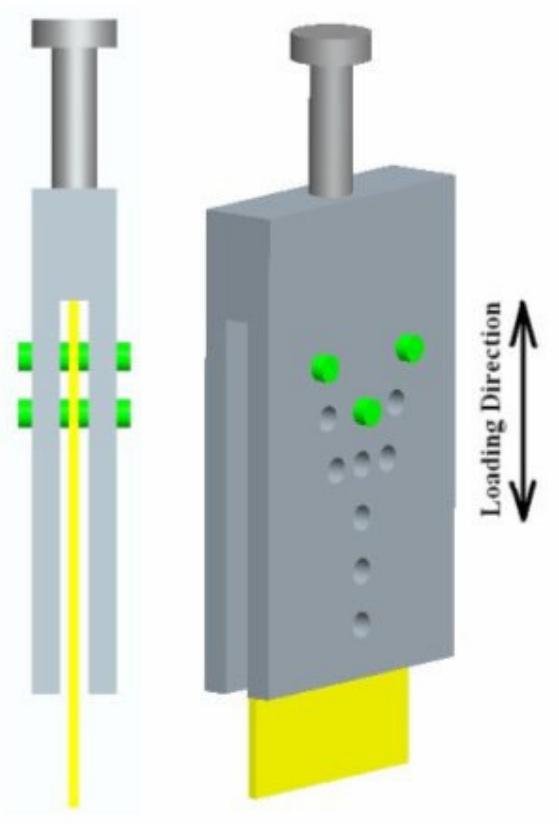

Figure 4.11 Tensile test setup – test fixture (grey), test specimen (yellow), and rigid pins (green)

CHAPTER FIVE

RESULTS AND DISCUSSION

In this study, maximum failure load and failure mode parameters were investigated experimentally and numerically. The specimens for each pin configuration were tested for experimental study. For the numerical study all pin configurations were modeled and analyzed by LUSAS 13.6 finite element analysis software. Geometric non-linear solution with Hashin failure criterion were selected for the numerical analysis.

Failure load values and failure modes were investigated for three variables, E/D ratio (1, 2, 3, 4, 5), F/D ratio (2, 4, 6), G/D ratio (3, 4, 5).

In the experimental study, load-displacement curves have been plotted and fixed E/D ratio-configurations were compared with each other respectively (Figure 5.1 to 5.5). It was seen that curves are linear before the initial failure (elastic region).

However, it was seen that the greater E/D ratio-configuration-specimens continued to carry the load up to 7 mm at nearly-constant load values.

Load vs. Pin-displacement diagrams can be seen below in Figure 5.1 to Figure 5.2 while;

- Figure 5.1, 5.2, 5.3, 5.4 & 5.5 indicate the change of G/D ratio.

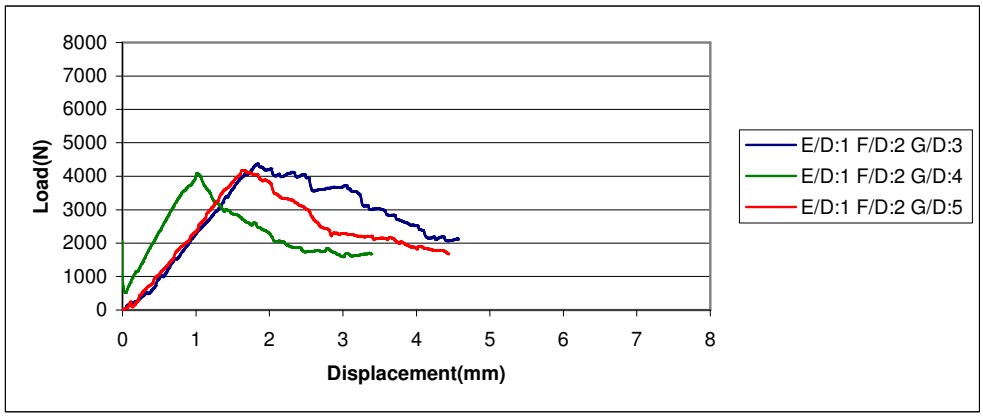

(a)

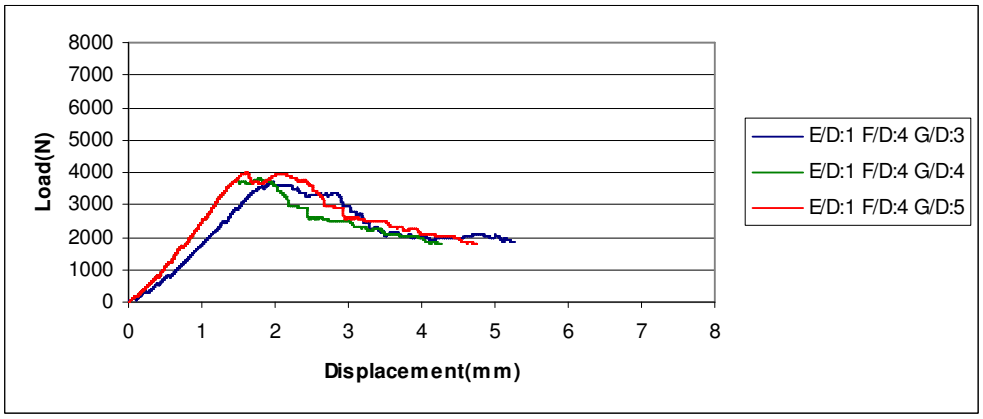

(b)

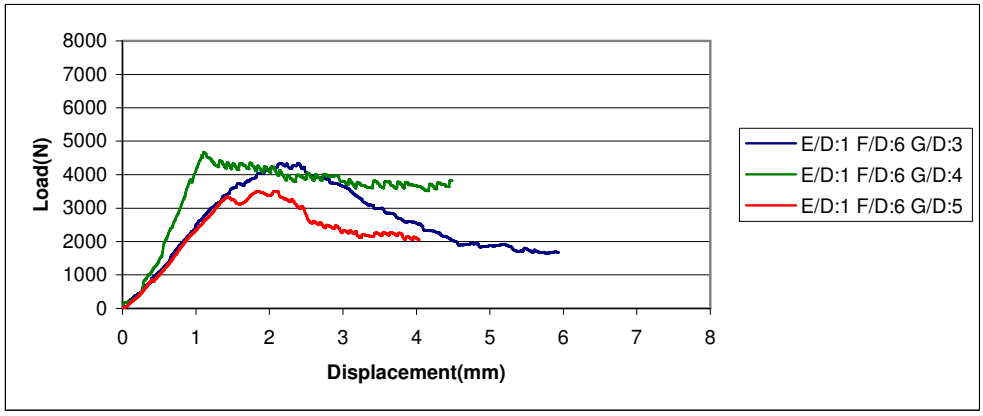

(c)

Figure 5.1 Load-Displacement curves of composite plates for E/D=1. (a) for F/D=2, (b) for F/D=4, (c)for F/D=6.

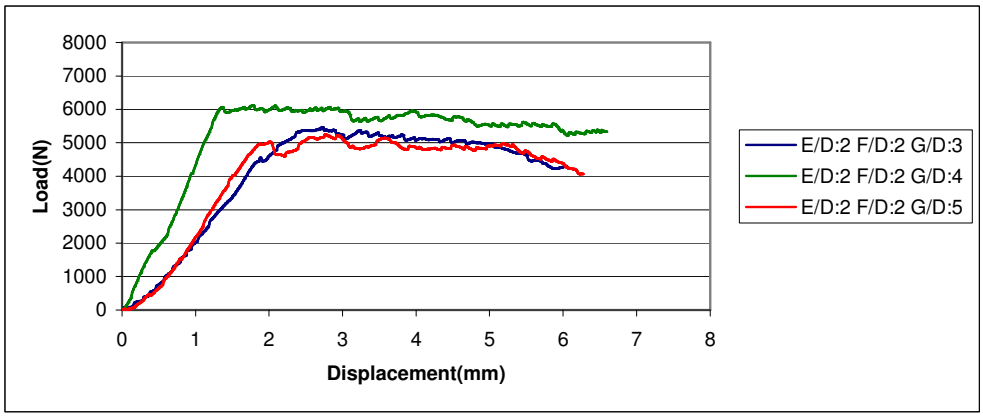

(a)

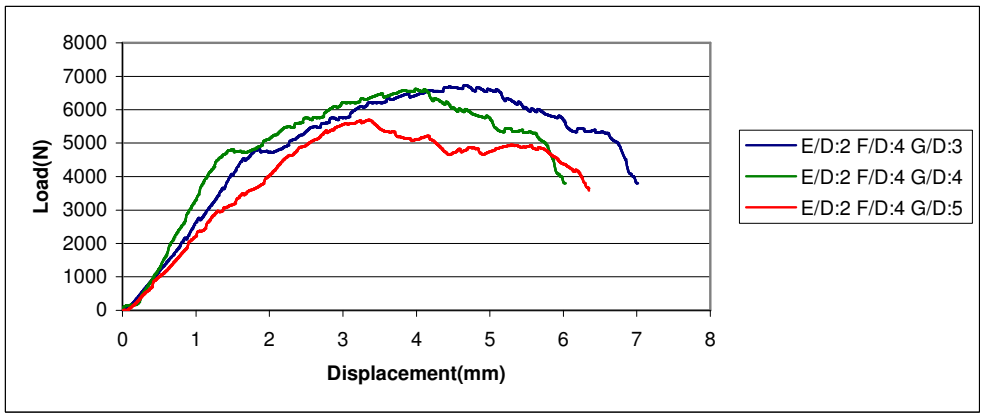

(b)

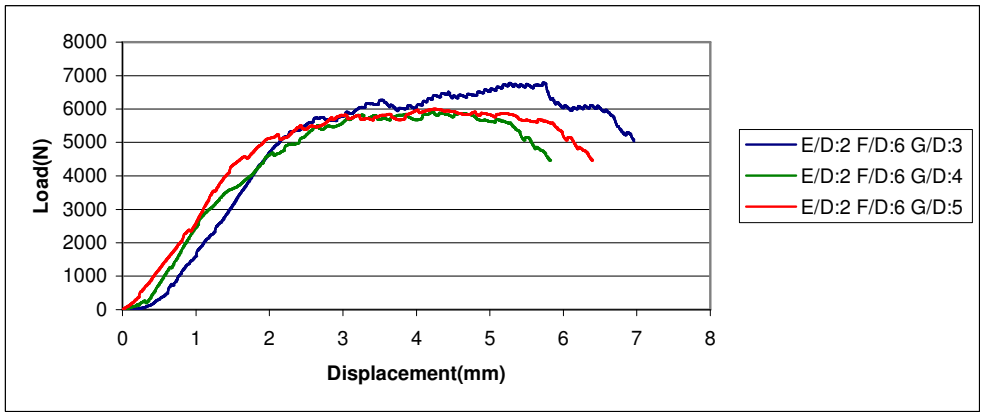

(c)

Figure 5.2 Load-Displacement curves of composite plates for E/D=2. (a) for F/D=2, (b) for F/D=4, (c) for F/D=6.

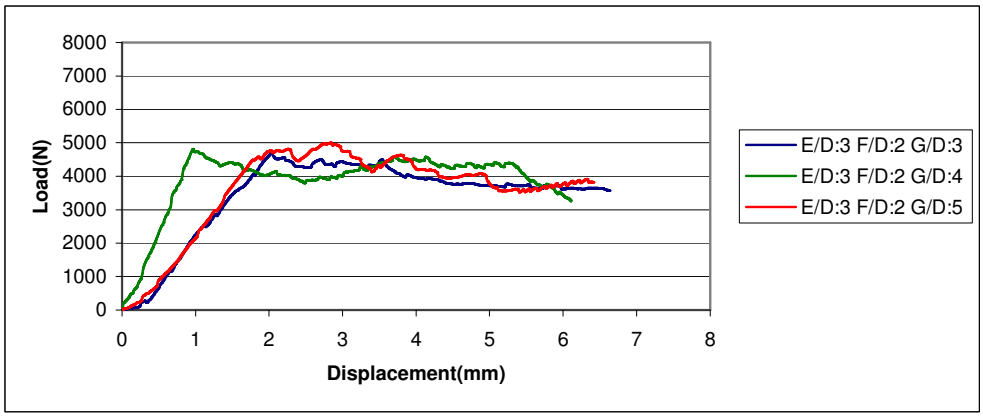

(a)

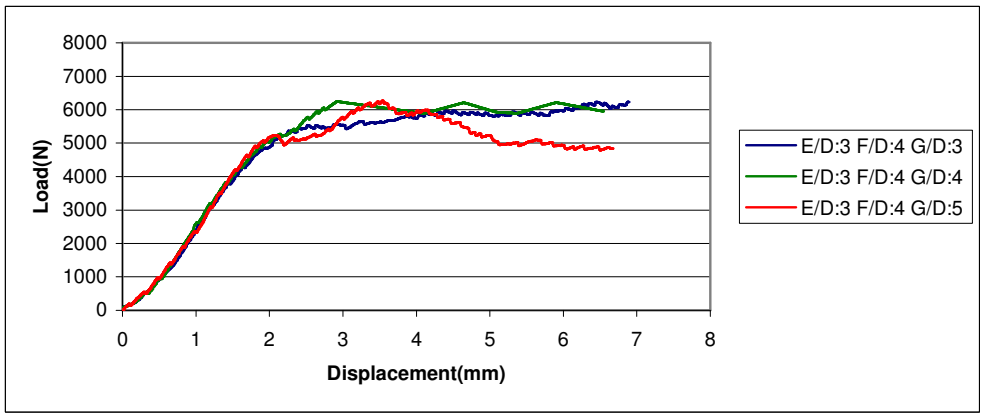

(b)

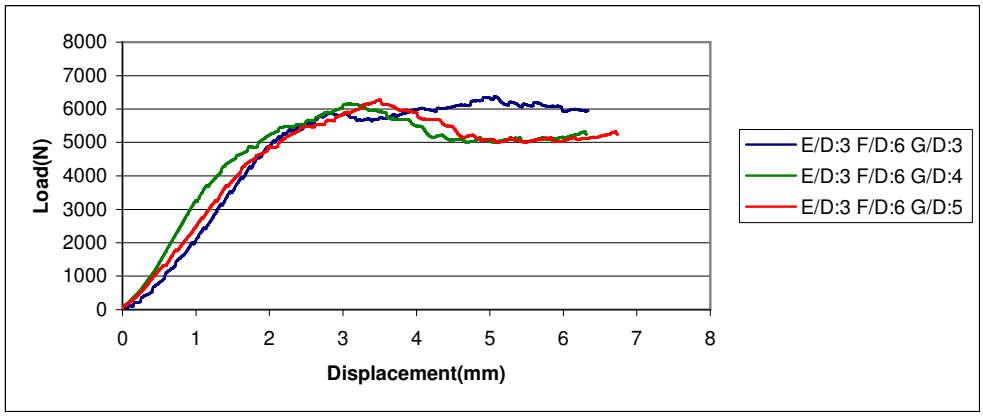

(c)

Figure 5.3 Load-Displacement curves of composite plates for E/D=3. (a) for F/D=2, (b) for F/D=4, (c) for F/D=6.

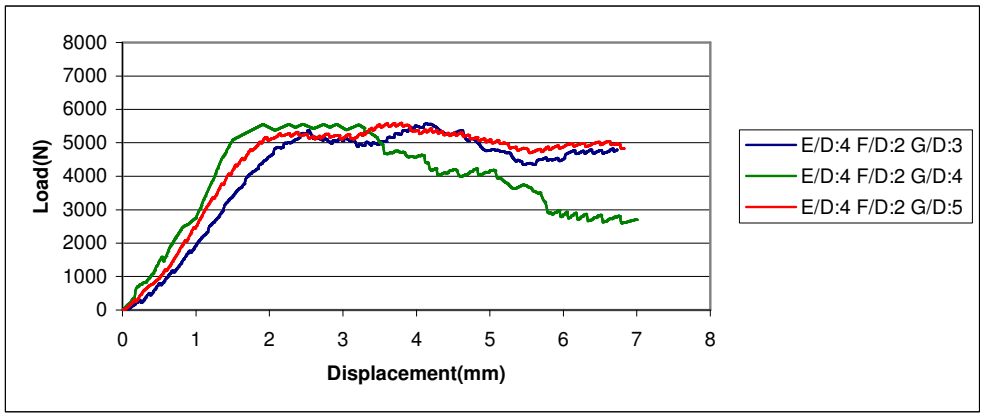

(a)

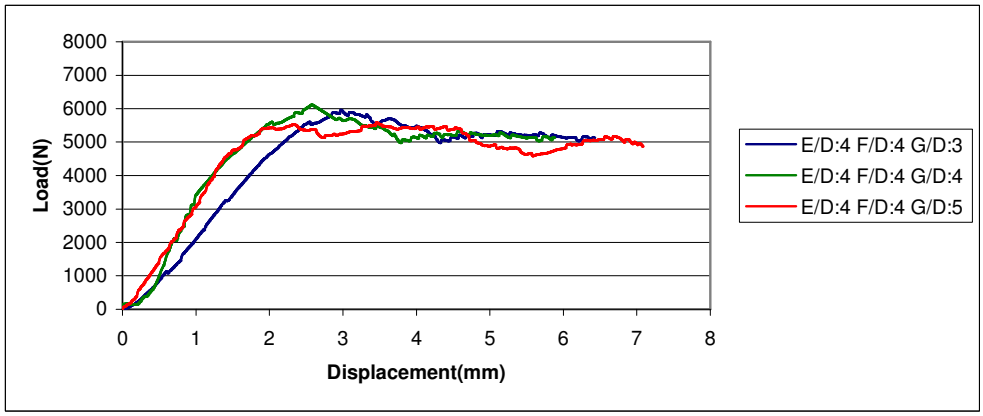

(b)

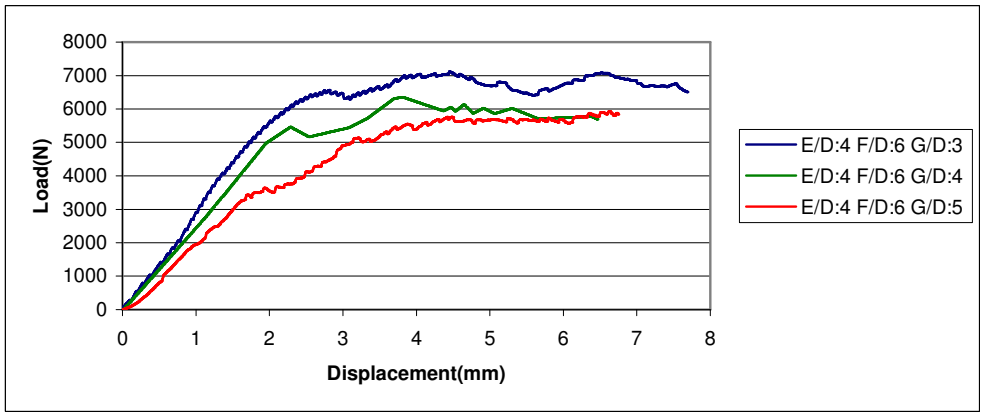

(c)

Figure 5.4 Load-Displacement curves of composite plates for E/D=4. (a) for F/D=2, (b) for F/D=4, (c) for F/D=6.

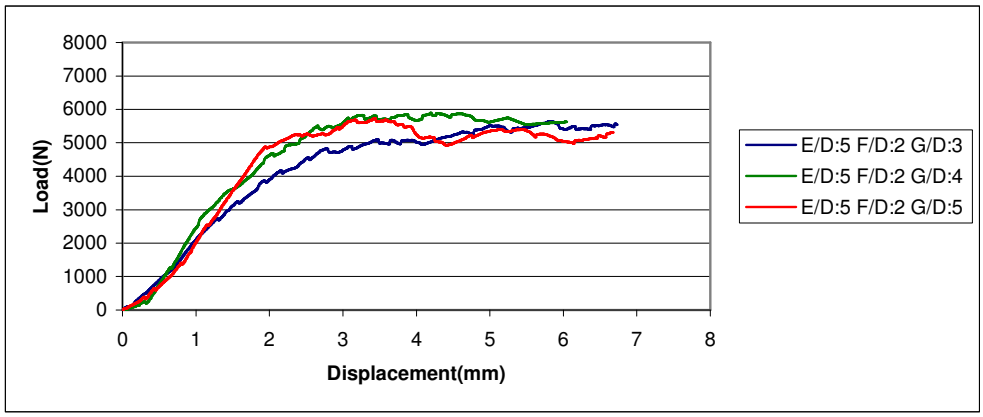

(a)

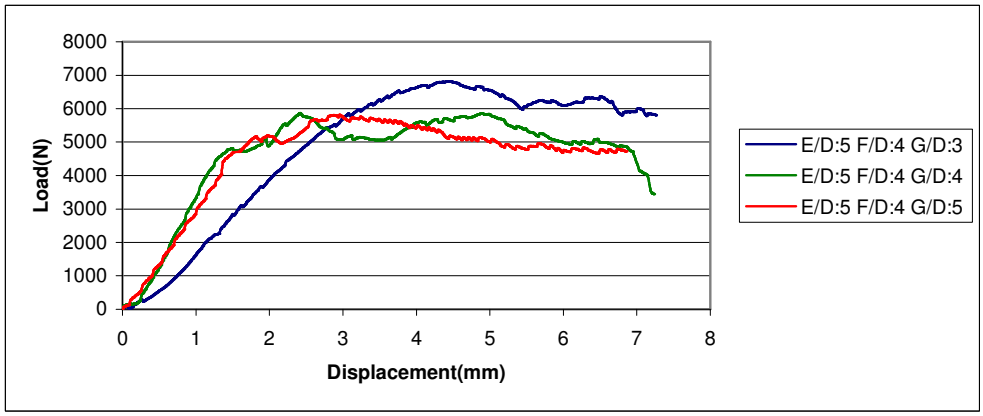

(b)

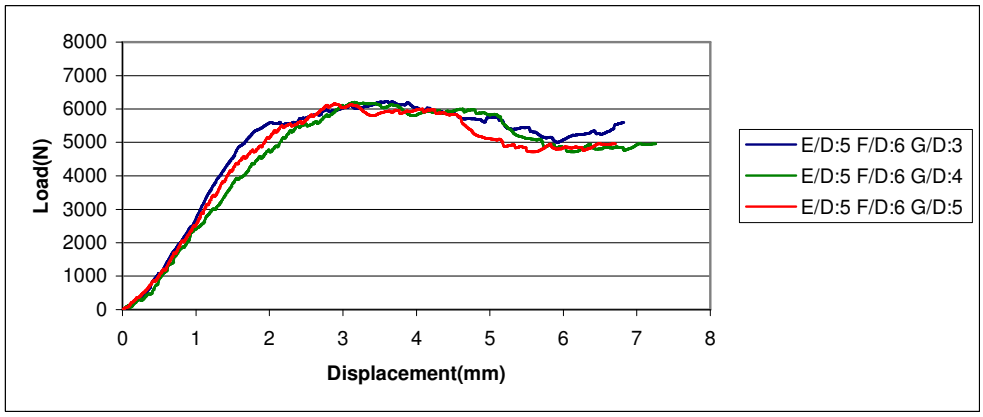

(c)

Figure 5.5 Load-Displacement curves of composite plates for E/D=5. (a) for F/D=2, (b) for F/D=4, (c) for F/D=6.

When we look at the failure modes, the lowest value of the E/D (E/D=1), have the combination of “Bearing” and “Shear-out” modes and also only “Shear-out” mode. As known that these are not secured modes, in practice the ratio of E/D=1 should not to be chosen. (Table 5.1)

At the same time, E/D=2 versions of the arrangements F/D=4, G/D=3 and F/D=4, G/D=4 have the failure mode of “Shear-out”, and the arrangement of F/D=4, G/D=5 and F/D=6, G/D=4 have the failure mode of “Bearing” and “Shear-out”, respectively. Although the configuration E/D=4, F/D=2, G/D=4 has the failure mode of “Shear-out”.

The remaining configurations have the “Bearing” mode, which is the most secured failure mode.

If we focused on the failure load values, these observations below can be determined:

The laminates that have the value of E/D=1 are the weakest configurations.

However, the configuration E/D=4, F/D=6, G/D=3 is the strongest and the most secured laminate.

Table 5.1 Results & comparisons of experimental with numerical failure loads and failure modes of the composite material (E/D=2)
(B = bearing mode, S = shear-out mode)

			Failure Load (N)		Failure Mode	
			Experimental	Numerical	Exp.	Num.
E / D = 1	F / D = 2	G / D = 3	4369	3200	S	S
		G / D = 4	4097	3800	S	S
		G / D = 5	4184	3406	S	S
	F / D = 4	G / D = 3	3700	2834	B-S	B-S
		G / D = 4	3825	3206	B-S	S
		G / D = 5	3999	2988	B-S	B
	F / D = 6	G / D = 3	4347	2544	S	B
		G / D = 4	4676	2684	S	B
		G / D = 5	3506	2713	B-S	B

Table 5.2 Results & comparisons of experimental with numerical failure loads and failure modes of the composite material (E/D=2)
(B = bearing mode, S = shear-out mode)

			Failure Load (N)		Failure Mode	
			Experimental	Numerical	Exp.	Num.
E / D = 2	F / D = 2	G / D = 3	5465	3838	B	S
		G / D = 4	6126	4500	B	S
		G / D = 5	5256	4669	B	S
	F / D = 4	G / D = 3	6729	3123	S	B-S
		G / D = 4	6620	3522	S	S
		G / D = 5	5697	3806	B-S	S
	F / D = 6	G / D = 3	6790	2728	B	B
		G / D = 4	5918	2945	B-S	B
		G / D = 5	6002	3016	B	B

Table 5.3 Results & comparisons of experimental with numerical failure loads and failure modes of the composite material (E/D=3)
(B = bearing mode, S = shear-out mode)

			Failure Load (N)		Failure Mode	
			Experimental	Numerical	Exp.	Num.
E / D = 3	F / D = 2	G / D = 3	4712	3838	B	S
		G / D = 4	4816	4578	B	S
		G / D = 5	5008	4568	B	S
	F / D = 4	G / D = 3	6233	3169	B	B
		G / D = 4	6246	3565	B	S
		G / D = 5	6273	4188	B	S
	F / D = 6	G / D = 3	6384	2749	B	B
		G / D = 4	6168	2988	B	B
		G / D = 5	6277	3063	B	B

Table 5.4 Results & comparisons of experimental with numerical failure loads and failure modes of the composite material (E/D=4)
(B = bearing mode, S = shear-out mode)

			Failure Load (N)		Failure Mode	
			Experimental	Numerical	Exp.	Num.
E / D = 4	F / D = 2	G / D = 3	5570	3877	B	B
		G / D = 4	5557	4514	B-S	S
		G / D = 5	5591	4500	B	S
	F / D = 4	G / D = 3	5956	3175	B	B
		G / D = 4	6120	3443	B	B
		G / D = 5	5588	4182	B	S
	F / D = 6	G / D = 3	7120	2763	B	B
		G / D = 4	6350	3342	B	S
		G / D = 5	5927	3319	B	S

Table 5.5 Results & comparisons of experimental with numerical failure loads and failure modes of the composite material (E/D=5)
(B = bearing mode, S = shear-out mode)

			Failure Load (N)		Failure Mode	
			Experimental	Numerical	Exp.	Num.
E / D = 5	F / D = 2	G / D = 3	5642	4075	B	B-S
		G / D = 4	5894	4550	B	S
		G / D = 5	5730	4300	B	B
	F / D = 4	G / D = 3	6820	3180	B	B
		G / D = 4	5867	3575	B	S
		G / D = 5	5814	3534	B	B
	F / D = 6	G / D = 3	6230	2769	B	B
		G / D = 4	6206	3319	B	S
		G / D = 5	6164	2698	B	B

"Failure Load" vs. "Hole Ratio" diagrams can be seen below in Figure 5.7 to 5.15 while;

- Figure 5.7 (a to c) indicates the experimental results of the effect of F/D ratio on the failure load while G/D changes
- Figure 5.8 (a to e) indicates the experimental results of the effect of G/D ratio on the failure load while E/D changes
- Figure 5.9 (a to c) indicates the numerical results of the effect of F/D ratio on the failure load while G/D changes
- Figure 5.10 (a to e) indicates the numerical results of the effect of G/D ratio on the failure load while E/D changes
- Figure 5.11, 5.12, 5.13, 5.14 & 5.15 indicate the experimental & numerical failure load values of the whole versions while E/D changes

When we focused on the results figure by figure these comments below can be written;

At G/D=3 in experimental results, for E/D=2 and E/D=5 the failure load values are nearly the same for each F/D. In addition, the maximum value occurred at the configuration of E/D=4, F/D=6. And also E/D=1 ratio has the weakest failure load values for each F/D. (Fig. 5.7.a)

At G/D=4 in experimental results, for E/D=4 and E/D=5 there are no remarkable changes of the failure load values for each F/D. And E/D=1 ratio has the lowest failure load values as the configuration of E/D=1 at G/D=3. (Fig. 5.7.b)

At G/D=5 in experimental results, for E/D=2, E/D=4 and E/D=5 there are no remarkable changes of the failure load values while F/D changes. For E/D=3, failure load values are linear for F/D=4 and F/D=6. And also E/D=1 ratio has the lowest failure load values as the configuration of G/D=3 and G/D=4. (Fig. 5.7.c)

So we can say that when we keep the G/D ratio constant, E/D=1 ratio has the lowest failure load values for each F/D.

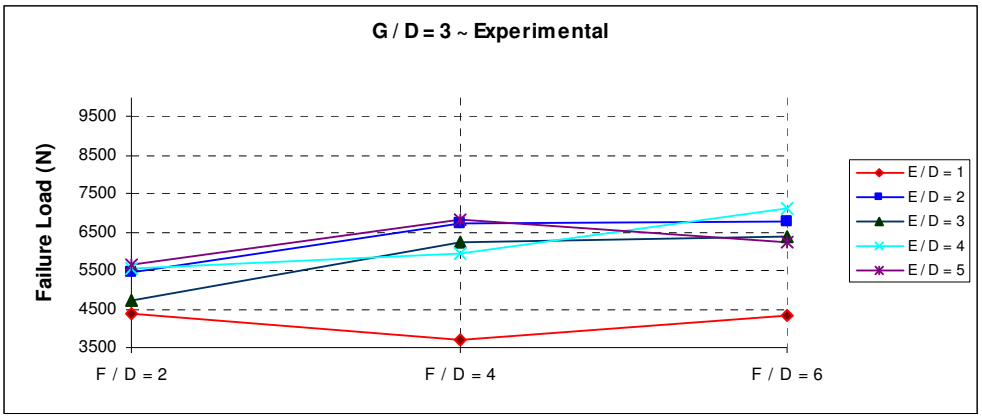

(a)

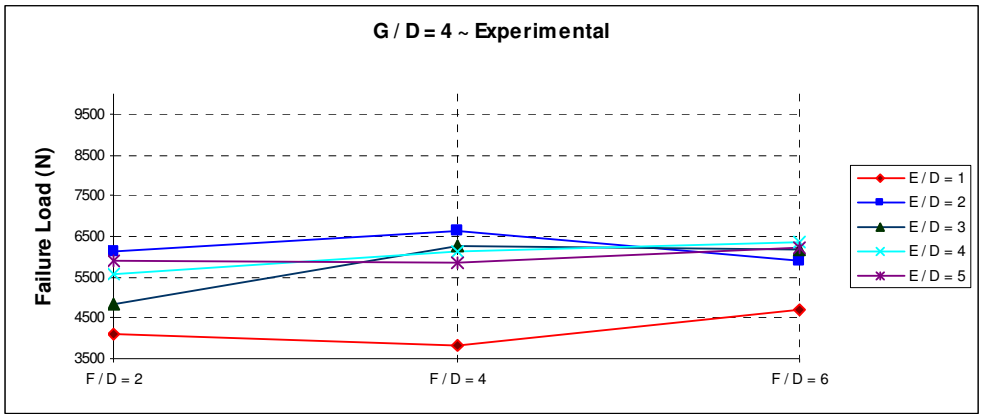

(b)

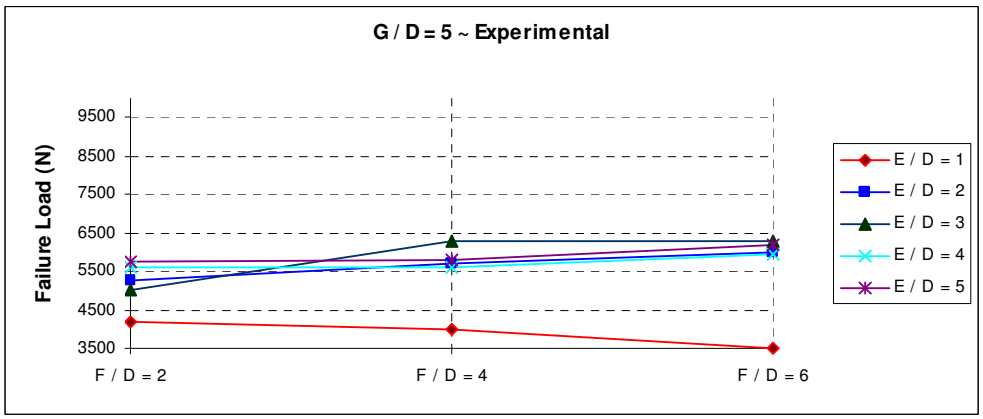

(c)

Figure 5.7 The experimental results of the effect of F/D ratio on the failure load (Change of G/D ratio, (a) for G/D=3, (b) for G/D=4, (c) for G/D=5)

At E/D=1 in experimental results, for F/D=2 failure load values are nearly same for G/D=4 and G/D=5. For F/D=4 failure loads are linear for each F/D. For F/D=6 failure loads are nearly same for G/D=3 and G/D=4. (Fig. 5.8.a)

At E/D=2 in experimental results, F/D=2 failure load values are nearly same for G/D=4 and G/D=5 and maximum failure load value in G/D=4 ratio. F/D=4 failure load values are nearly same for G/D=3 and G/D=4. (Fig. 5.8.b)

At E/D=3 in experimental results, the failure loads goes linearly for each F/D. For F/D=4 and F/D=6, failure load values are same. And also F/D=2 has the lowest failure load values. (Fig. 5.8.c)

At E/D=4 in experimental results, F/D=2 failure load values are same for each G/D. F/D=6 failure values decrease linearly. (Fig. 5.8.d)

At E/D=5 in experimental results, for F/D=2 and F/D=6 failure loads are on linear line. And also F/D=2 and F/D=4 have the same failure load values at G/D=4 and G/D=5. (Fig. 5.8.e)

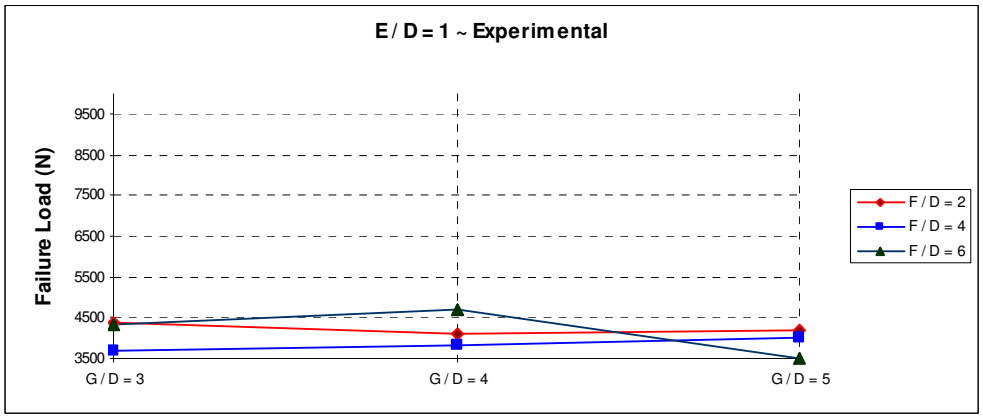

(a)

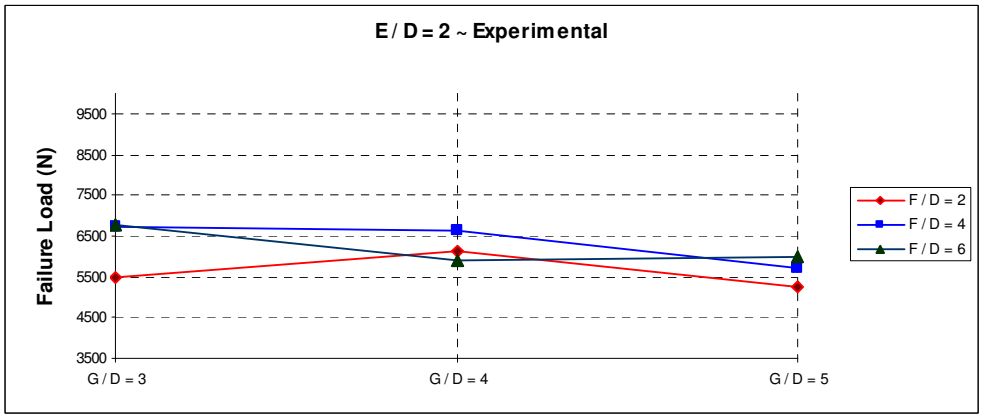

(b)

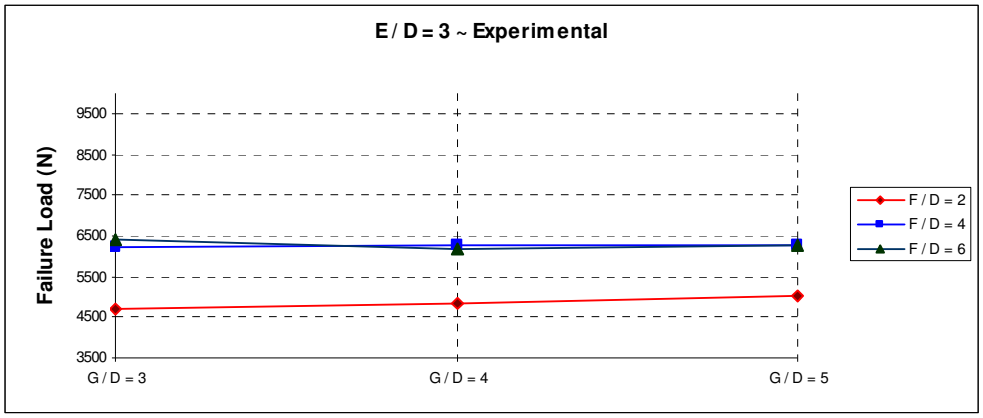

(c)

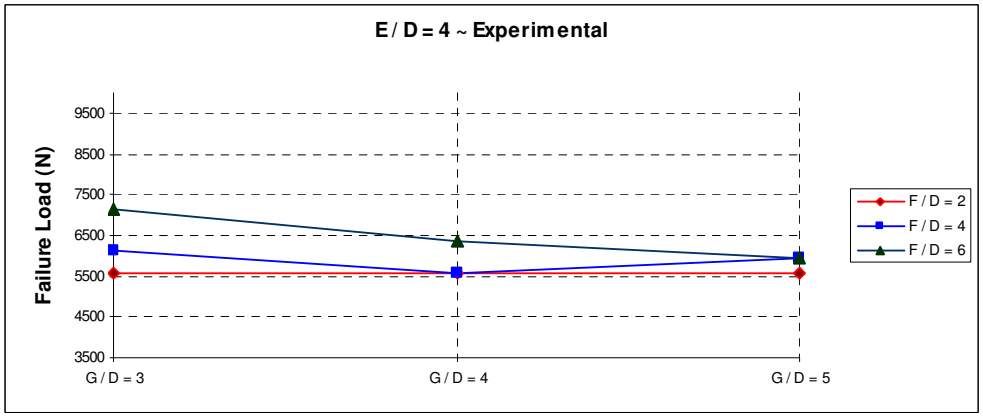

(d)

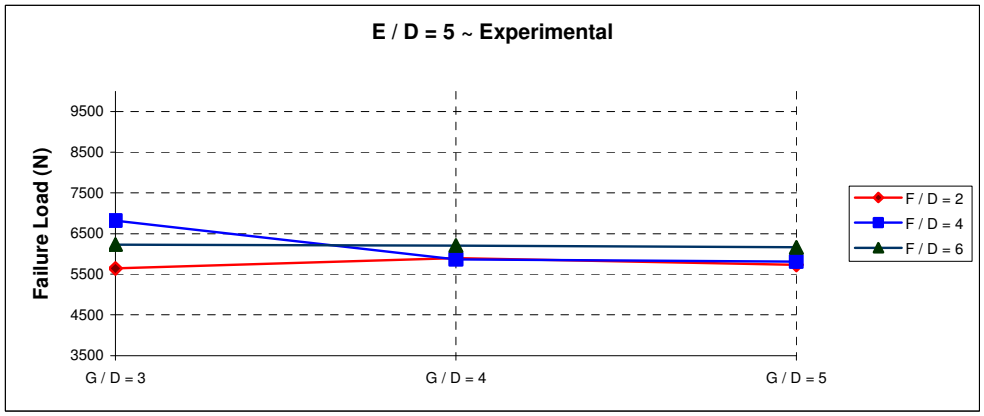

(e)

Figure 5.8 The experimental results of the effect of G/D ratio on the failure load (Change of E/D ratio, (a) for E/D=1, (b) for E/D=2, (c) for E/D=3, (d) for E/D=4, (e) for E/D=5)

At experimental result of E/D=1, the minimum failure load value occurred at maximum values of G/D and F/Ds. The failure load tended to stay linearly while G/D increase for F/D=2 and F/D=4. (Fig.5.11.a)

At numerical result of E/D=1, the maximum failure load occurred at G/D=4 as same as experimental results but in opposition to experimental result at the minimum value of F/D=2. (Fig.5.11.b)

At experimental result of E/D=2, the minimum failure load value occurred at the maximum value of G/D and the minimum value of F/Ds. The maximum failure load value occurred at minimum value of G/D and maximum value of F/D. The failure load tended to decrease while G/D increased and F/D decreased. (Fig.5.12.a)

At numerical result of E/D=2, in opposition to experimental values the minimum failure load value occurred at the minimum value of G/D and the maximum value of F/Ds. The maximum failure load value occurred at maximum value of G/D and minimum value of F/D. The failure load tended to decrease while G/D decreased and F/D increased. (Fig.5.12.b)

At experimental result of E/D=3, the minimum failure load value occurred at three region of min F/D. The maximum failure load value occurred at minimum value of G/D and maximum value of F/D. The failure load tended to keep its linearity for F/D=4 and F/D=6. (Fig.5.13.a)

At numerical result of E/D=3, the minimum failure load value occurred at two region of max F/D. The maximum failure load value occurred at minimum value of minimum value of F/D. (Fig.5.13.b)

At experimental result of E/D=4, the minimum failure load value occurred at four regions, the three of them at the minimum values of F/Ds, the other one is at the configuration of F/D=4, G/D=5. The maximum failure load value occurred at minimum value of G/D and maximum value of F/D. The failure load tended to decrease while G/D increased and F/D decreased. (Fig.5.14.a)

At numerical result of E/D=4, the minimum failure load value occurred at the minimum values of G/D and the maximum values of F/Ds. The maximum failure load value occurred at maximum value of G/D and minimum value of F/D. The failure load tended to increase while G/D and F/D increased. (Fig.5.14.b)

At experimental result of E/D=5, the maximum failure load value occurred at F/D=4, G/D=3. For F/D=2 and F/D=4, except this maximum failure load value, the other failure load values stay linearly as minimum failure load values.. And also the failure load values belong to F/D=6 keep their linearity by themselves. (Fig.5.15.a)

At numerical result of E/D=5, the maximum failure load value occurred at F/D=2, G/D=4. For F/D=4, the failure load values are same for G/D=4 and G/D=5. And also the minimum failure load value occurred at the maximum values of F/D. (Fig.5.15.b)

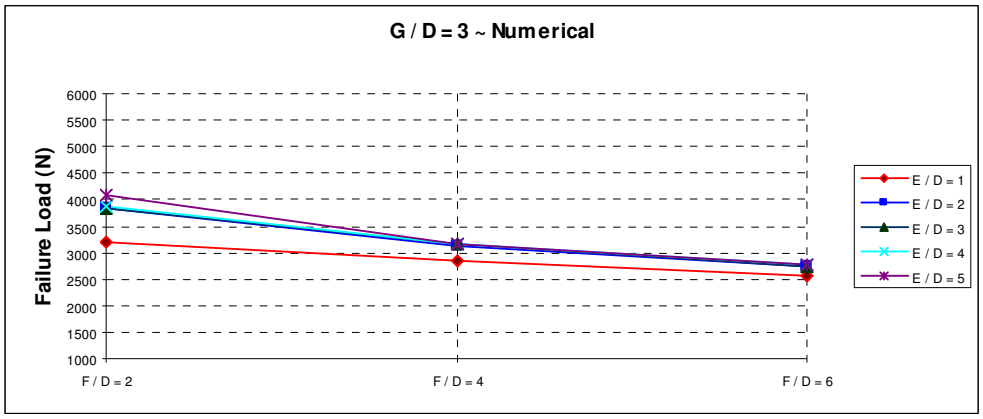

(a)

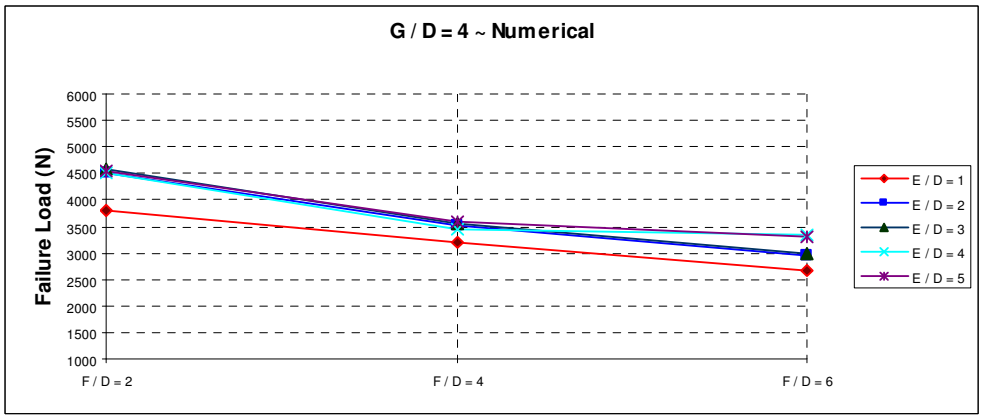

(b)

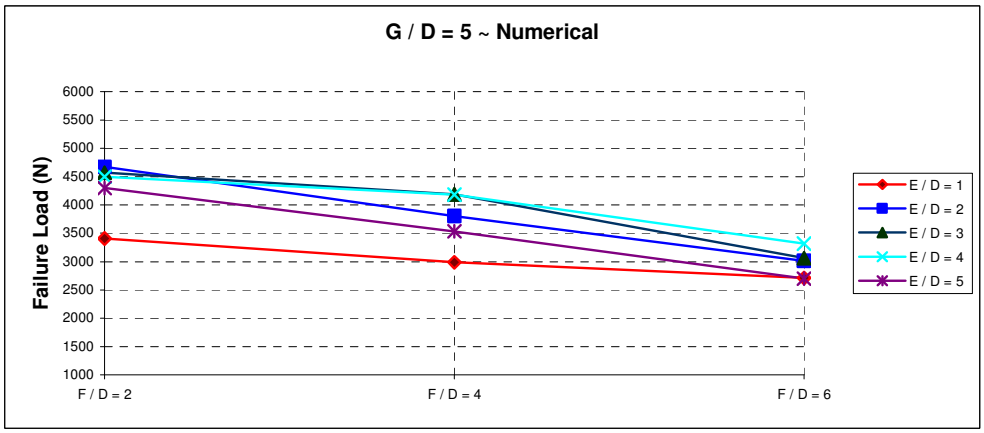

(c)

Figure 5.9 The numerical results of the effect of F/D ratio on the failure load. (Change of G/D ratio, (a) for G/D=3, (b) for G/D=4, (c) for G/D=5)

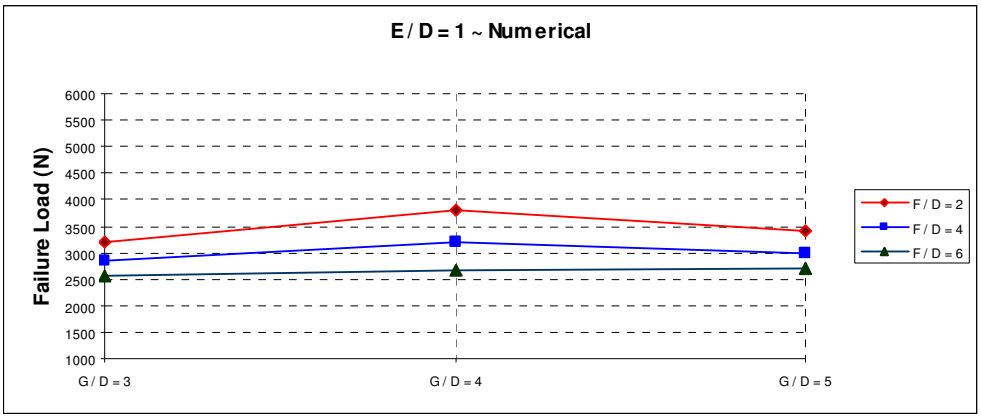
E / D = 1 ~ Numerical
Failure Load (N)
6000
5500
5000
4500
4000
3500
3000
2500
2000
1500
1000
G / D = 3
G / D = 4
G / D = 5
F / D = 2
F / D = 4
F / D = 6

(a)

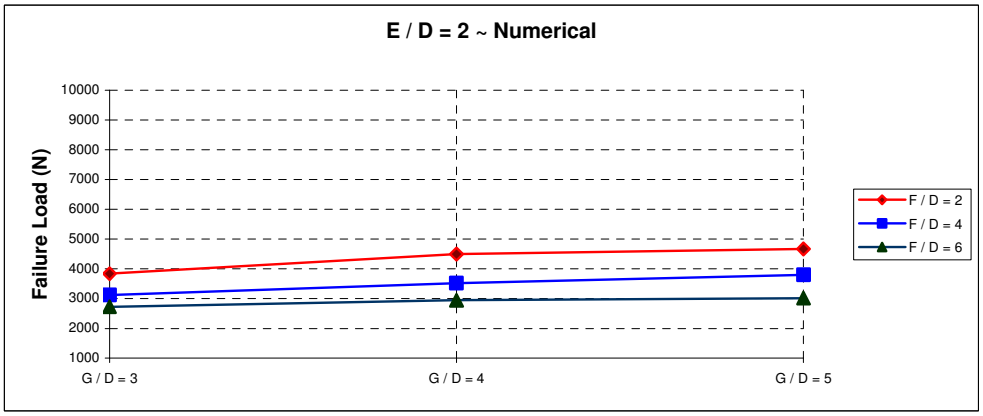
E / D = 2 ~ Numerical
Failure Load (N)
10000
9000
8000
7000
6000
5000
4000
3000
2000
1000
G / D = 3
G / D = 4
G / D = 5
F / D = 2
F / D = 4
F / D = 6

(b)

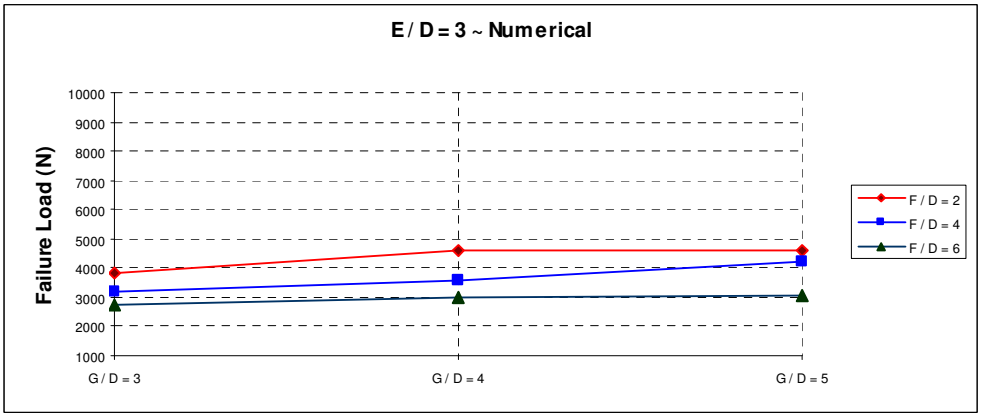
E / D = 3 ~ Numerical
Failure Load (N)
10000
9000
8000
7000
6000
5000
4000
3000
2000
1000
G / D = 3
G / D = 4
G / D = 5
F / D = 2
F / D = 4
F / D = 6

(c)

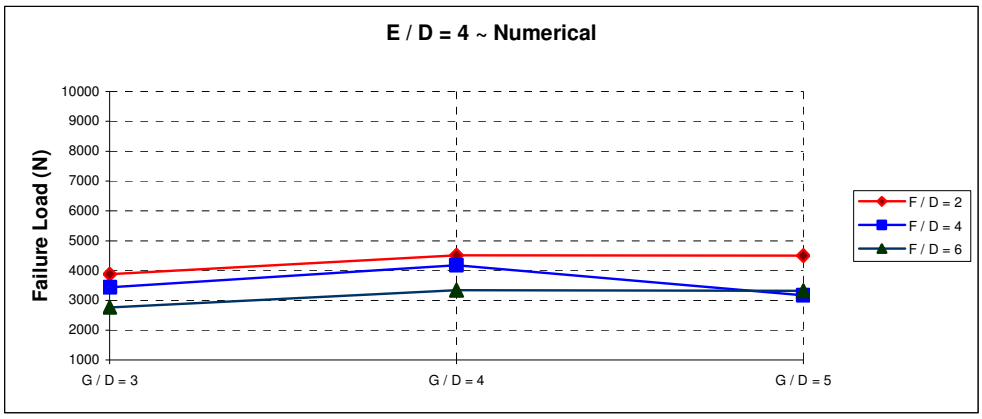

(d)

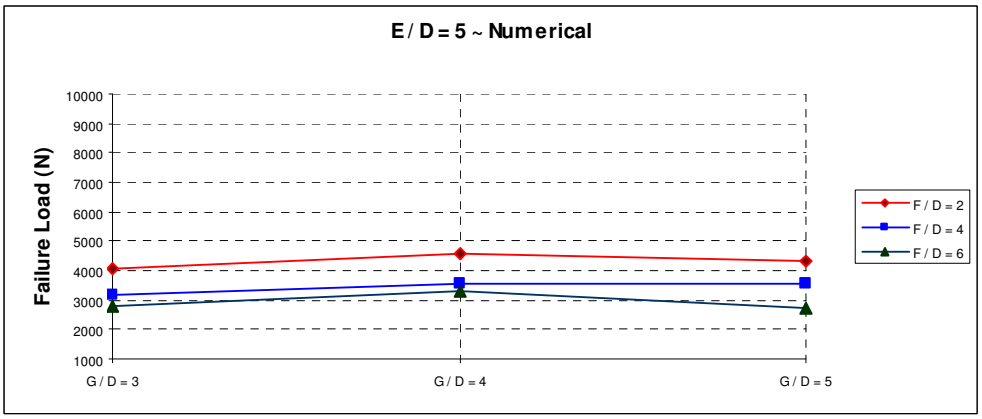

(e)

Figure 5.10 The numerical results of the effect of G/D ratio on the failure load (Change of E/D ratio, (a) for E/D=1, (b) for E/D=2, (c) for E/D=3, (d) for E/D=4, (e) for E/D=5)

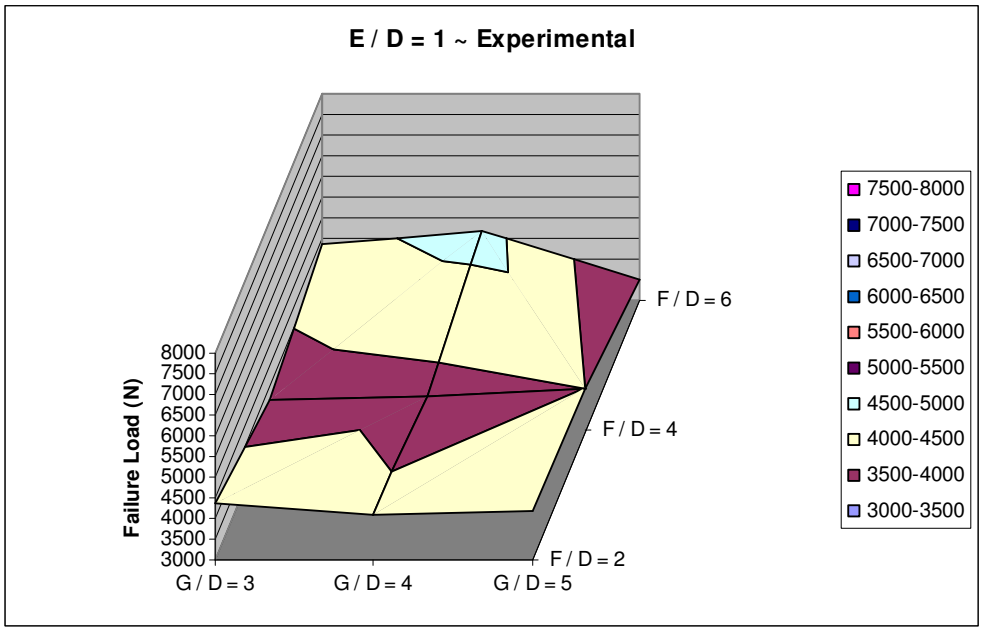

(a)

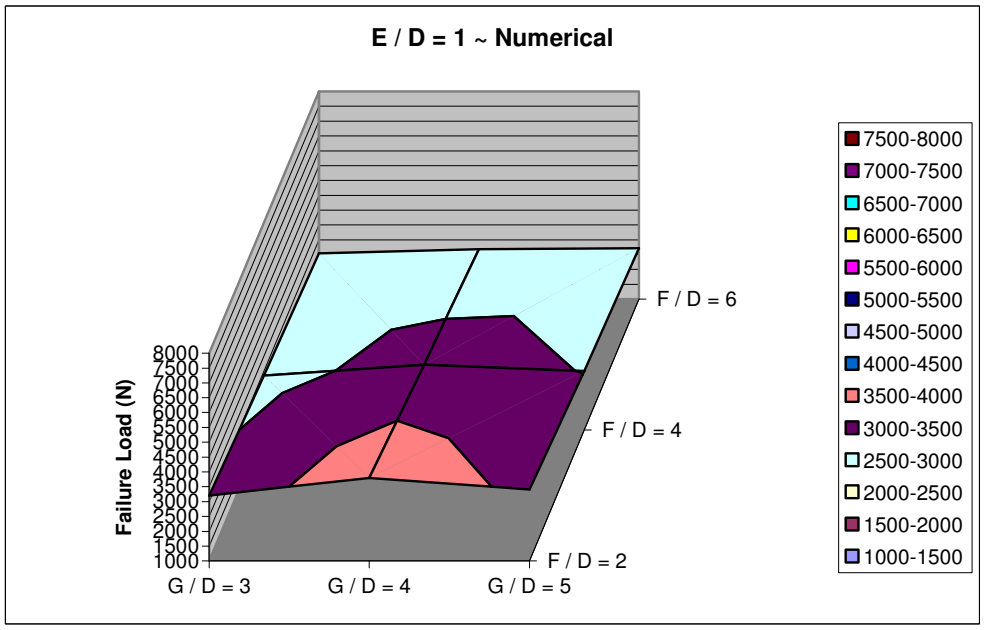

(b)

Figure 5.11 The experimental & numerical results of the composite plates with E/D=1. (a) for experimental results and (b) for numerical results.

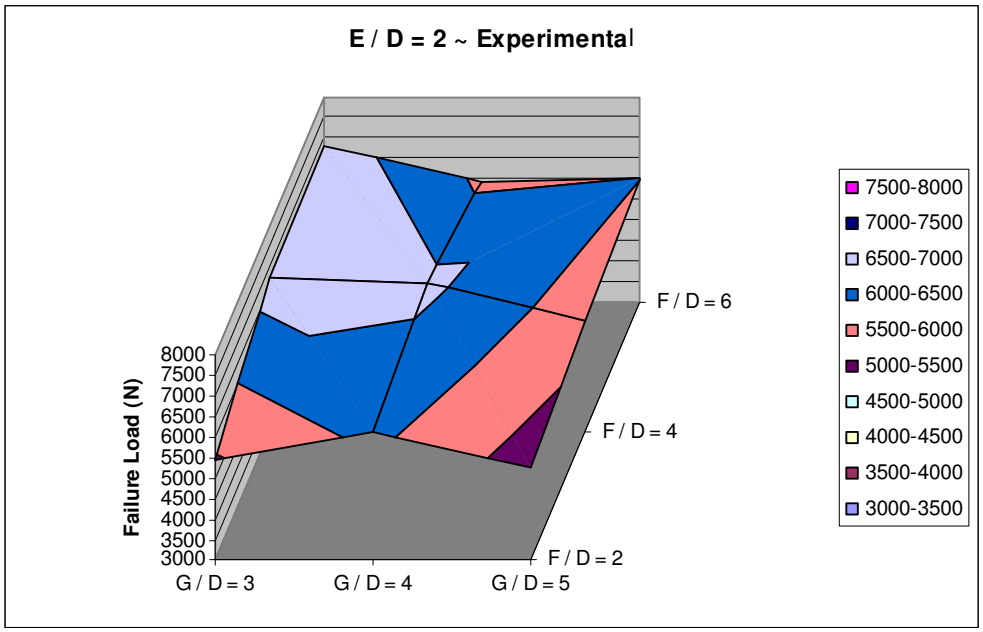

(a)

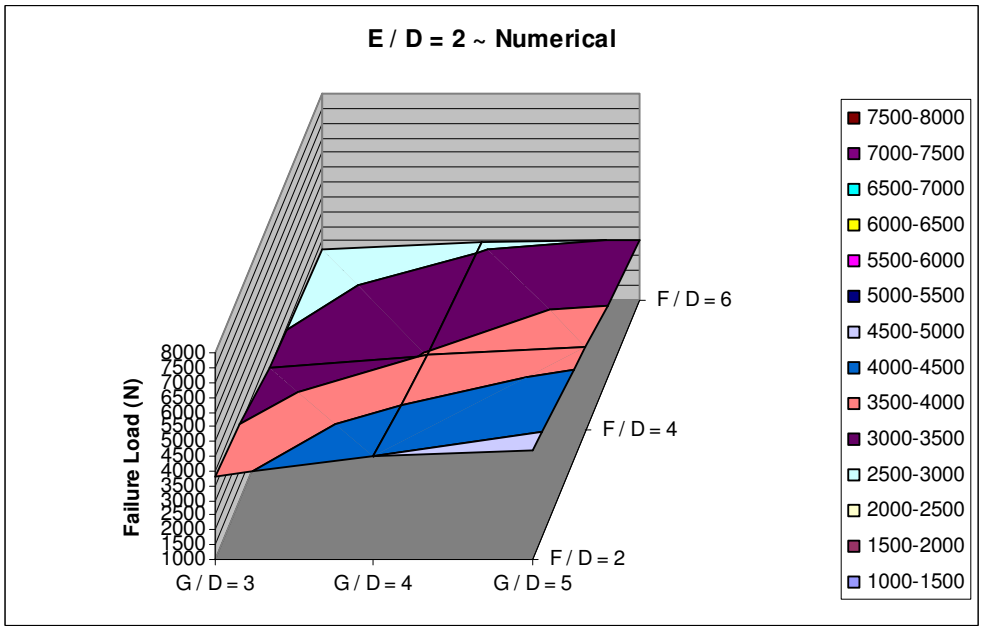

(b)

Figure 5.12 The experimental & numerical results of the composite plates with E/D=2. (a) for experimental results and (b) for numerical results.

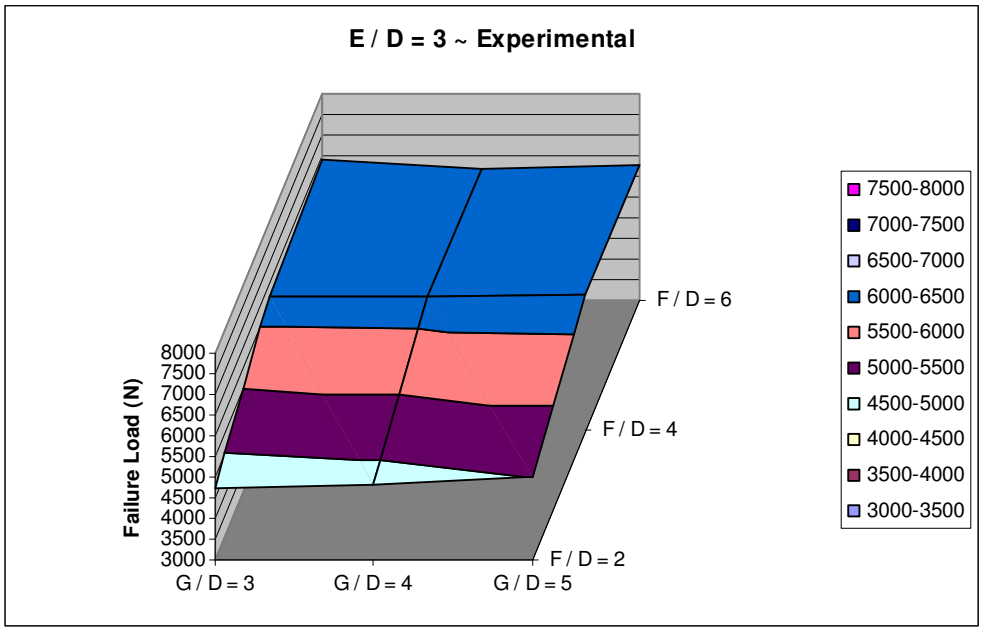

(a)

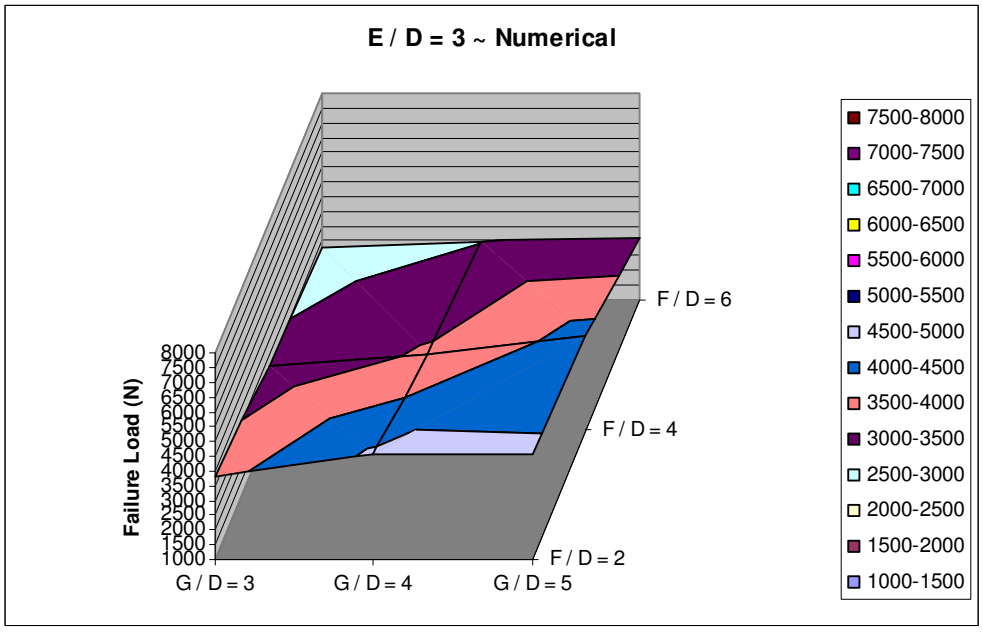

(b)

Figure 5.13 The experimental & numerical results of the composite plates with E/D=3. (a) for experimental results and (b) for numerical results.

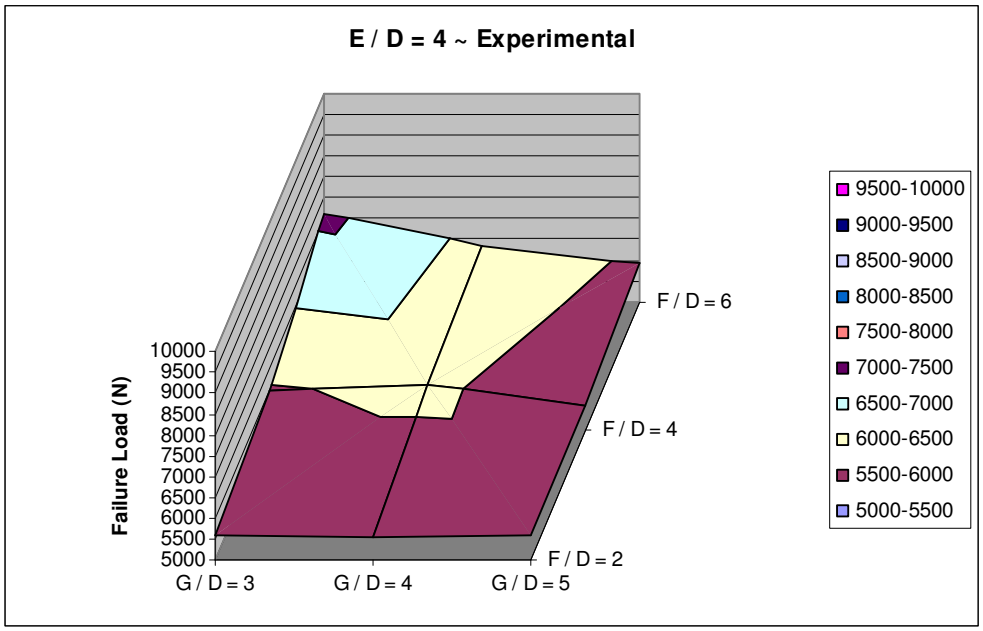

(a)

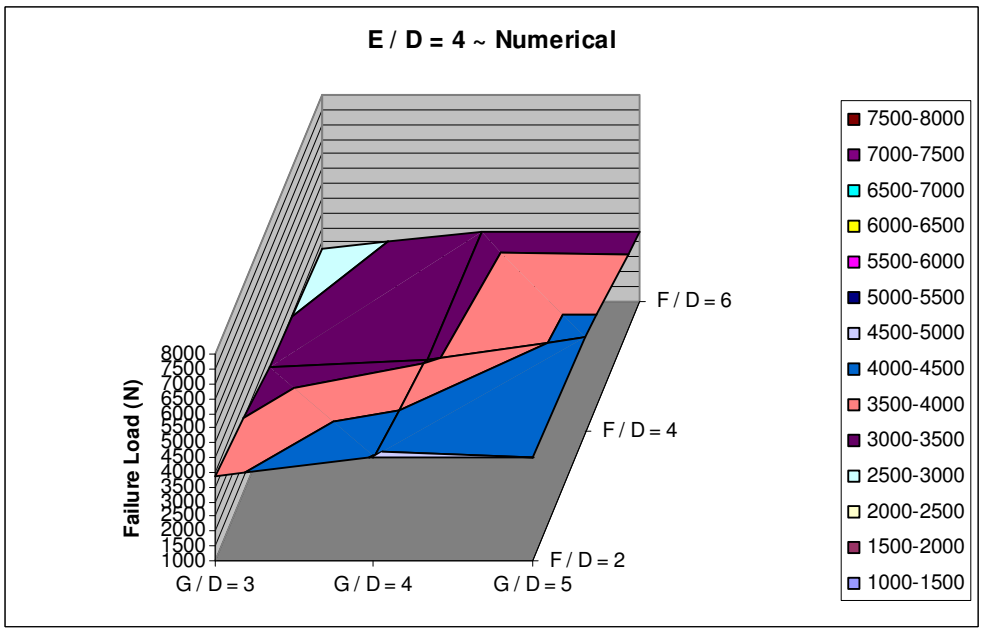

(b)

Figure 5.14 The experimental & numerical results of the composite plates with E/D=4. (a) for experimental results and (b) for numerical results.

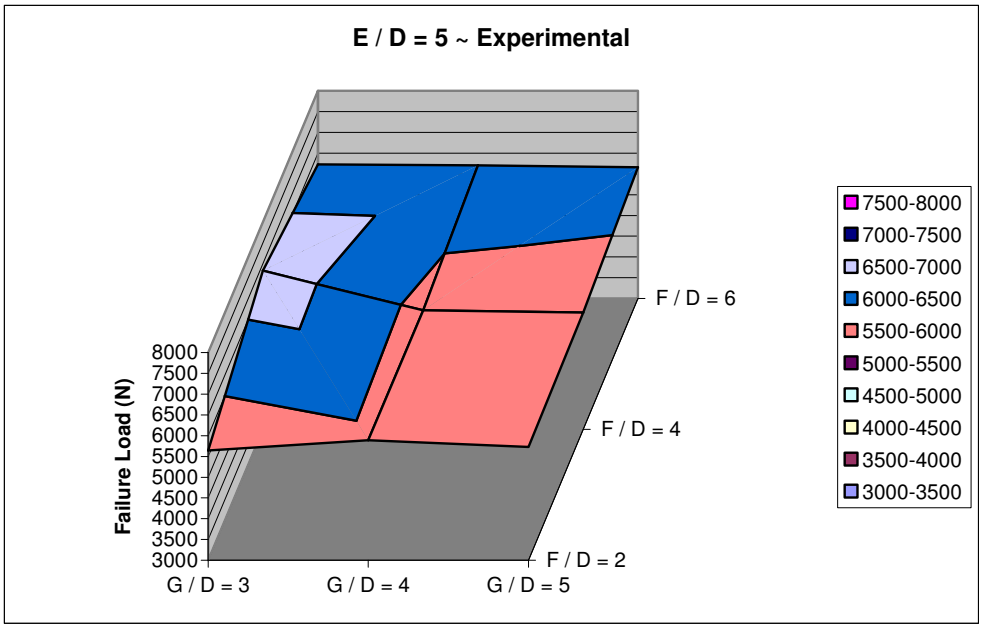

(a)

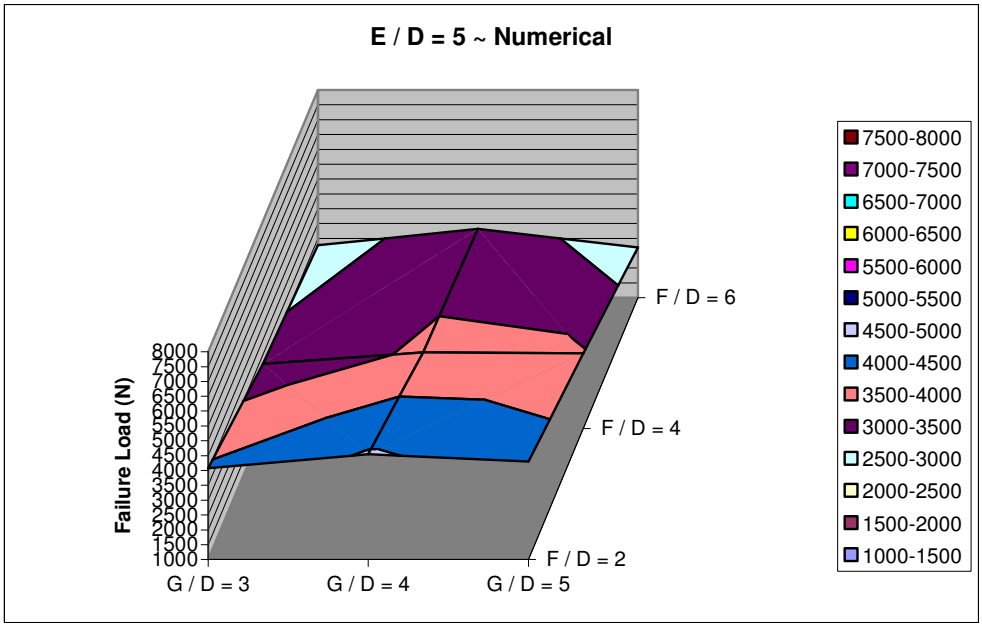

(b)

Figure 5.15 The experimental & numerical results of the composite plates with E/D=5. (a) for experimental results and (b) for numerical results.

The contours below are the couple of samples of the numerical study. The red regions below indicate that failure occurs since the Hashin failure criteria values are greater than 1.

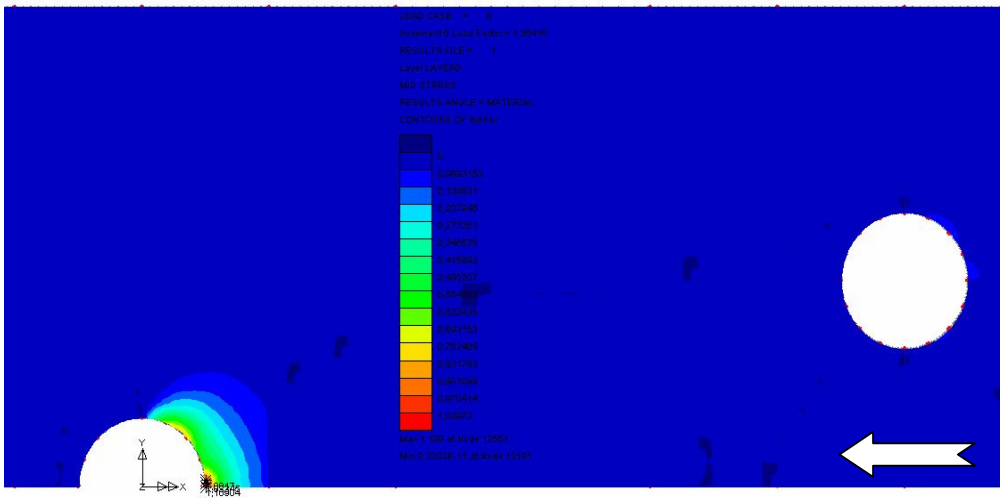

Figure 5.16 Numerical study - Hashin failure criteria of the configuration E/D=2,F/D=6,G/D=3

(x indicates the region which failure has been occurred with respect to Hashin failure criteria, the failure mode is “Bearing”, failure load is 2728N)

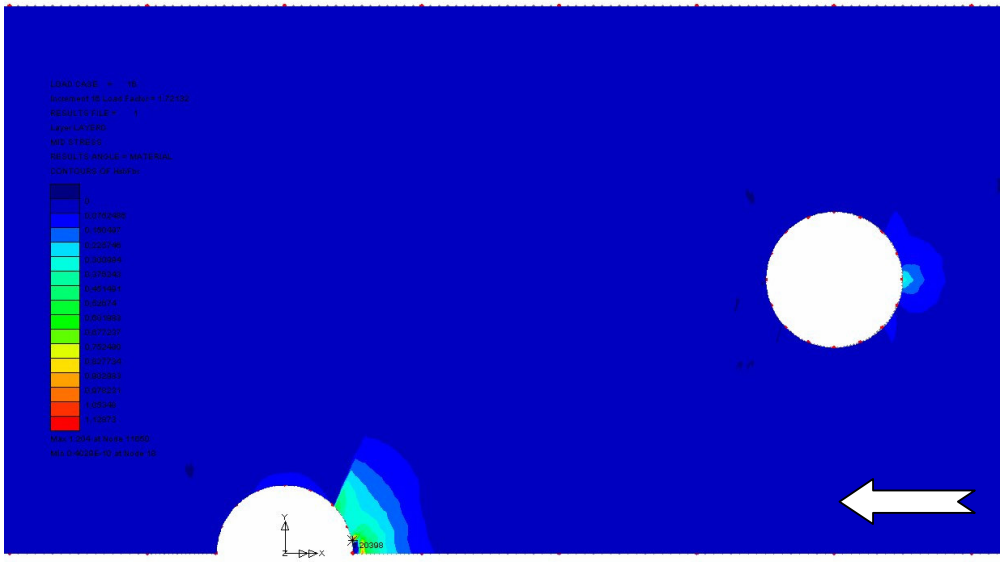

Figure 5.17 Numerical study - Hashin failure criteria of the configuration E/D=4,F/D=4,G/D=4

(x indicates the region which failure has been occurred with respect to Hashin failure criteria, the failure mode is “Bearing”, failure load is 3443 N)

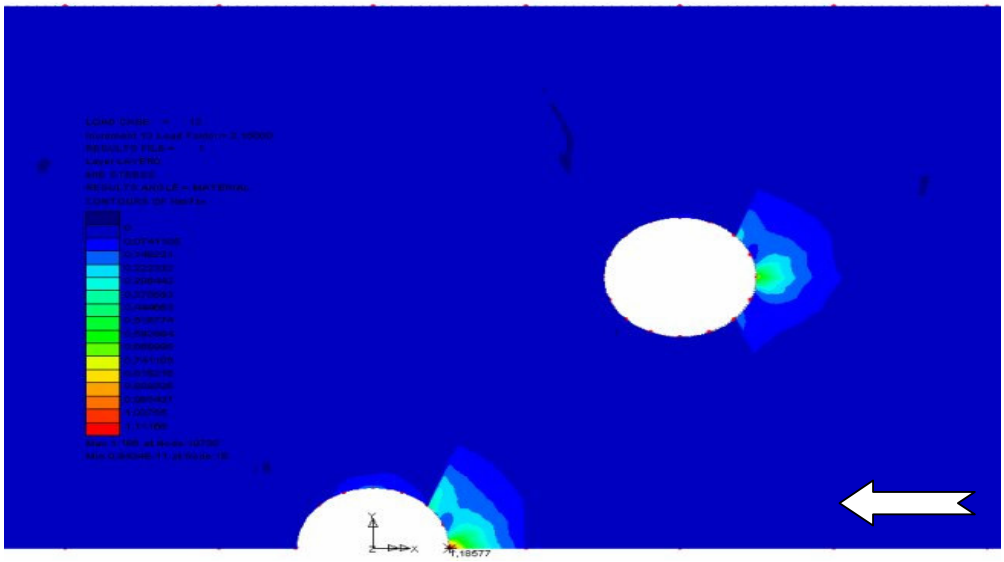

Figure 5.18 Numerical study - Hashin failure criteria of the configuration E/D=5,F/D=2,G/D=5

(x indicates the region which failure has been occurred with respect to Hashin failure criteria, the failure mode is “Bearing”, failure load is 4300 N)

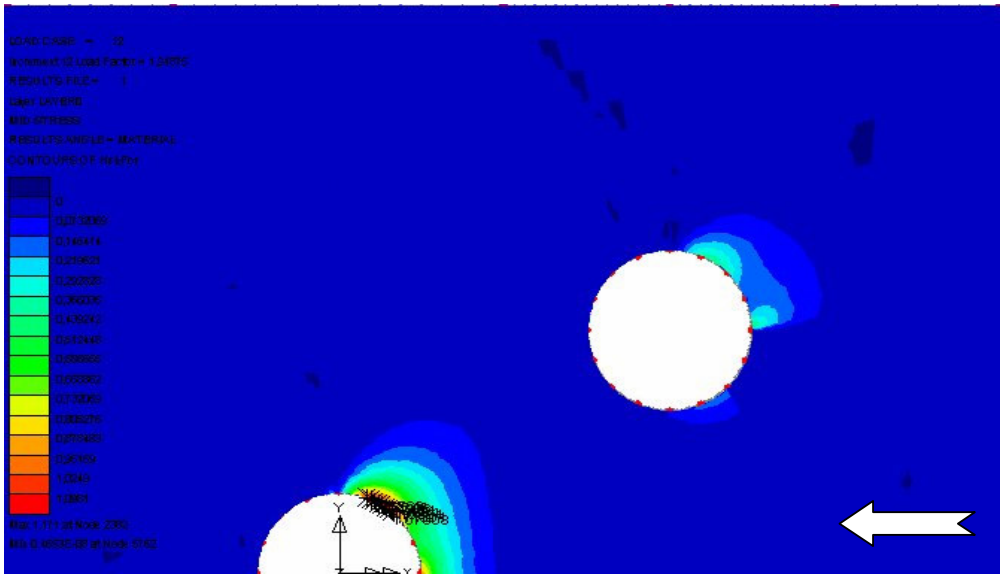

Figure 5.19 Numerical study - Hashin failure criteria of the configuration E/D=2,F/D=2,G/D=3

(x indicates the region which failure has been occurred with respect to Hashin failure criteria, the failure mode is “Shear-Out”, failure load is 3838 N)

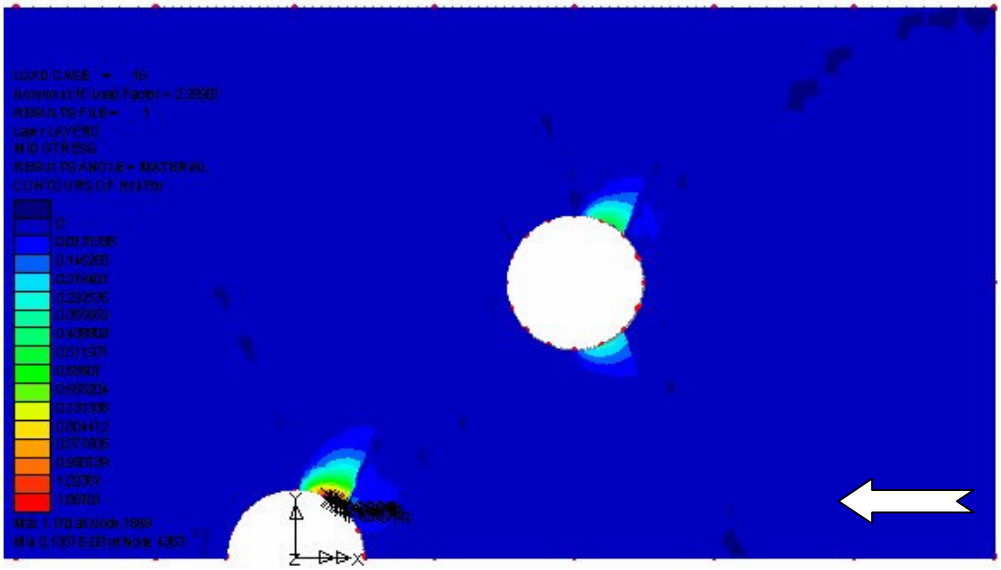

Figure 5.20 Numerical study - Hashin failure criteria of the configuration E/D=3,F/D=2,G/D=4
(x indicates the region which failure has been occurred with respect to Hashin failure criteria,
the failure mode is “Shear-Out”, failure load is 4578 N)

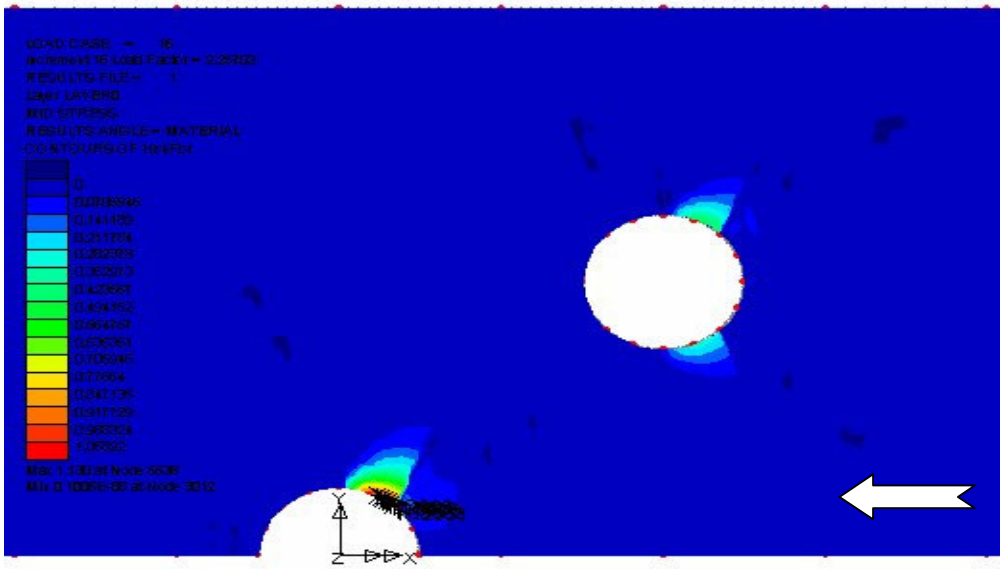

Figure 5.21 Numerical study - Hashin failure criteria of the configuration E/D=4,F/D=2,G/D=4
(x indicates the region which failure has been occurred with respect to Hashin failure criteria,
the failure mode is “Shear-Out”, failure load is 4514 N)

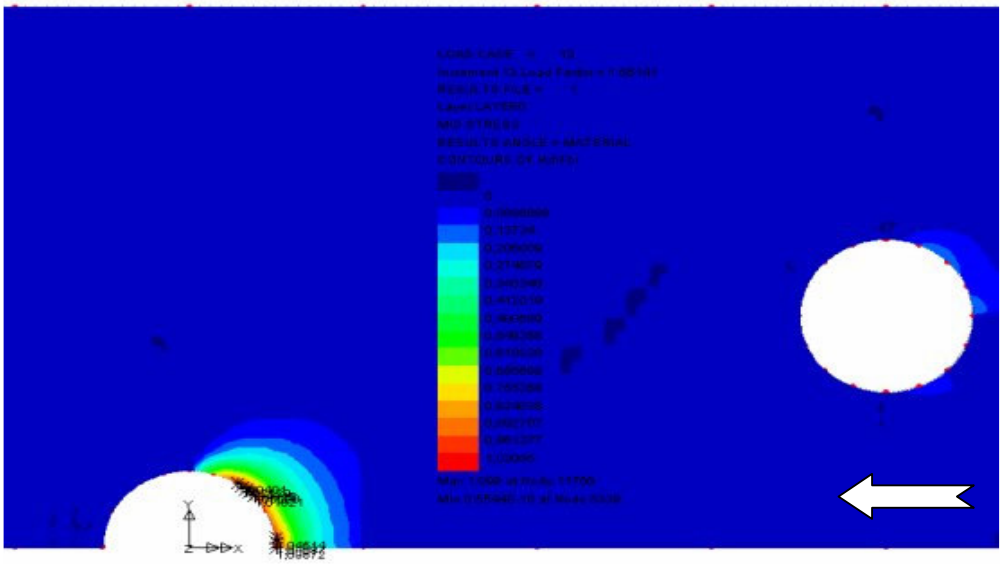

Figure 5.22 Numerical study - Hashin failure criteria of the configuration E/D=2,F/D=4,G/D=3
(x indicates the region which failure has been occurred with respect to Hashin failure criteria, the failure mode is “Bearing + Shear-Out”, failure load is 3123 N)

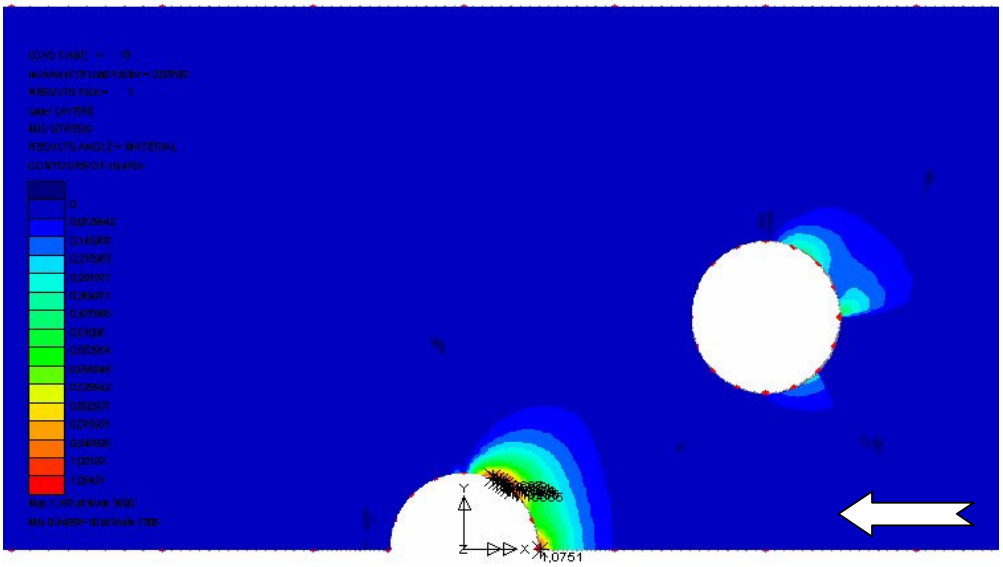

Figure 5.23 Numerical study - Hashin failure criteria of the configuration E/D=5,F/D=2,G/D=3
(x indicates the region which failure has been occurred with respect to Hashin failure criteria, the failure mode is “Bearing + Shear-Out”, failure load is 4075 N.

CHAPTER SIX

CONCLUSIONS

In this study, “failure load” and “failure mode” parameters were investigated experimentally and numerically. The specimens for each pin configuration were tested for experimental study. For the numerical study all pin configurations were modeled and analyzed by LUSAS 13.6 finite element analysis software. Geometric non-linear solution with Hashin failure criterion were selected for the numerical analysis. Failure load values and failure modes were investigated for three variables, E/D ratio (1,2,3,4,5), F/D ratio (2,4,6), G/D ratio (3,4,5). In both the experimental and numerical studies, “Load-Displacement” and “Failure Load-Hole Distance Ratio” curves have been plotted and compared with each other.

It was seen that curves are linear before the initial failure (elastic region). It can be say that most of the specimens were reached the failure loads between the displacements of 1 and 3 mm.

However, it was seen that the greater E/D ratio-configuration-specimens continued to carry the load up to7 mm at nearly-constant load values.

When we look at the failure modes of all , the lowest value of the E/D (E/D=1), have the “Shear-out” and the “Bearing + Shear-out” modes. And also some of the combinations of E/D=2 has the failure modes of “Shear-out” and the “Bearing + Shear-out” modes. As known that these are not secured modes, in practice the ratio of E/D=1 and E/D=2 should not to be chosen.

At the same time, for the version of the arrangement E/D=4, F/D=2, G/D=8 the same failure mode “Bearing + Shear-out”, occurred.

The remaining configurations had the “Bearing” mode, which is the most secured failure mode.

In experimental results, it was seen that the failure load tend to increase while the E/D and F/D ratios increase. So the laminates which have the higher values of E/D and F/D ratios should be chosen. But this rule is not valid for G/D ratio. The failure load values are not depend on this ratio in this study.

The configuration E/D=4, F/D=6, G/D=3 has the maximum failure load value and it is the strongest and the most secured laminate in experimental results. But in numerical results, this configuration has very low failure load value.

The configuration E/D=1, F/D=6, G/D=5 has the minimum failure load value and it is the weakest laminate in experimental results.

In numerical analysis, the maximum failure load occurred at the version of E/D=2, F/D=2, G/D=5 and the minimum failure load value occurred at the version of E/D= 1, F/D=6, G/D=3.

REFERENCES

Akkuş A. (2005) Bearing strength of carbon epoxy laminates under static and dynamic loading. *Composite Structures* 67, 485-489.

Aktaş A, & Karakuzu R., (1998) Failure Analysis of Two Dimensional Carbon-Epoxy Composite Plate Pinned-Joint, *Proc. NATO Advanced Study Institute on Mechanics of CompositeMaterials and Structures*, 12–24 July 1998, Troia, Portugal, vol. 3, pp. 381–397, IDMEC/IST, Lisbon, Portugal.

Aktaş A, Karakuzu R. (1999) Failure analysis of two-dimensional carbon–epoxy composite plate pinned joint. *Mech Compos Mater Struct*;6:347–61.

B. L. Larry and M. S. Mahmood, (1995) Two DimensionalModeling of Composite Pinned-Joint Failure, *J. Composite Mater*, vol. 29, pp. 671–696.

Camanho, P.P, & Matthews, F.L. (1999). A Progressive Damage Model for Mechanically Fastened Joints in Composite Laminates. *Journal of Composite Materials*, 33, 2248-2280

Chang FK, Scott RA, Springer GS. (1982) Strength of mechanically fastened composite joints. *J Comp Mater*;16:470–94.

Chang, F.K. (1983). Strength of bolted joints in laminated composites. *Unpublished Ph.D. Dissertation, University of Michigan*

Chang, F.K., Scott, R.A., & Springer, G.S. (1984)a. Failure of Composite Laminates Containing Pin Loaded Holes- Method and Solution. *Journal of Composite Materials*, 18, 255-278.

Chang, F.K., Scott, R.A., & Springer, G.S. (1984)b. Failure Strength of Nonlinearly Elastic Composite Laminates Containing a Pin Loaded Hole. *Journal of Composite Materials*, 18, 464-477.

Chen JC, Chiu CH, Chin H. (1994) On the influence of weave structure on pin-loaded strength of orthogonal 3D composites. *J Comp Mater*;30:251–62.

Chun M., Niu Y., (1992), *Composite Airframe Structures: Practical Design information and Data*, Florida: Conmilit Pres Ltd.

Dano, M.L., Gendron, G., & Picard, A. (2000). Stress and Failure Analysis of Mechanically Fastened Joints in Composite Laminates. *Composite Structures*, 50, 287-296

Hassan, N.K., Mohamedien, M.A., & Rizkalla, S.H. (1996). Finite element analysis of bolted connections for PFRP composites. *Composites: Part B, 27B*, 339-349.

Icten BM, Okutan B, Karakuzu R. (2003) Failure strength of woven glass fiber–epoxy composites pinned joints. *J Compos Mater*;37:1337–51.

İçten B.M., Karakuzu R.& Toygar M.E., (2006)b Failure analysis of woven kevlar fiber reinforced epoxy composites pinned joints. *Composite Structures*, 73, 443–450

Jones R.M., (1999), Mechanics of Composite Materials, (2nd Ed.), USA: Taylor&Francis, Inc.

Karakuzu R., Gülem T., İçten B.M. (2006)a. Failure analysis of woven laminated glass-vinylester composites with pin-loaded hole. *Composite Structures, 72, 27-32*

Kretsis G, Matthews FL. (1985) The strength of bolted joints in glass fibre/epoxy laminates. *J Compos Mater*;16:92–102.

Lekhnitskii SG. (1968) *Anisotropic plates (English edition).* London:Gordon and Beach; (Translated by S.W. Tsai and T.Cheron).

Liu D, Raju BB, You J. (1999) Thickness effects on pinned joints for composites. *J Comp Mater*;33:2–21.

M. Ozbay, (1998) Buckling of Laminated Plates with Semicircular Holes, *J. Inst. Sci. Technol. Gazi Univ.*, vol. 10, pp. 393–401.

M. S. Mahmood and B. L. Larry, (1996) Effects of Material Nonlinearity on the Three-Dimensional Stress State of Pin-Loaded Composite Laminates, *J. Composite Mater.*, vol. 30, pp. 839–861.

Matthews F.L., Davies G.A.O., Hitchings D. & Soutis C. (2000) *Finite element modelling of composite materials and structures*, Cambridge: Woodhead Publishing Ltd. and CRC Press LLC.

Mazumdar, S.K., (2002) *Composites manufacturing : materials, product, and process Engineering*, USA: CRC Press LLC

Okutan B., Aslan Z., Karakuzu R., (2001) A study of the effects of various geometric parameters on the failure strength of pin-loaded woven-glass-fiber reinforced epoxy laminate*, Composites Science and Technology*, 61, 1491–1497.

Okutan, B., Aslan, Z., & Karakuzu, R. (2001). A Study of The Effects of Various Geometric Parameters On The Failure Strength of Pin-Loaded Woven-Glass-Fiber Reinforced Epoxy Laminate. *Composite Science and Technology*, 61, 1491-1497

Okutan B., Karakuzu R., (2003) The strength of pinned joints in laminated composites, *Composites Science and Technology*, 63, 893–905.

.Wang D.**,** Gang C., Zhengneng L. & Changhe K. (2006). Bearing Strength Analysis of Single Mechanically Fastened Joint in Stitched Laminates. *Journal of Reinforced Plastics and Composites 25, 711-724*

Whitney JM, Nuismer RJ. (1974) Stress fracture criteria for laminated composites containing stress concentrations. *J Mater*;8:253–65.